IEEE Access
Multidisciplinary | Rapid Review | Open Access Journal

Received September 17, 2020, accepted September 24, 2020, date of publication September 29, 2020,
date of current version October 14, 2020.

Digital Object Identifier 10.1109/ACCESS.2020.3027524

Optimal Planning of Nuclear-Renewable Micro-Hybrid Energy System by Particle Swarm Optimization

HOSSAM A. GABBAR[1,2], (Senior Member, IEEE), MUHAMMAD R. ABDUSSAMI[1], AND MD. IBRAHIM ADHAM[1]

[1]Faculty of Energy Systems and Nuclear Science, Ontario Tech University, Oshawa, ON L1G 0C5, Canada
[2]Faculty of Engineering and Applied Science, Ontario Tech University, Oshawa, ON L1G 0C5, Canada

Corresponding author: Hossam A. Gabbar (hossam.gabbar@uoit.ca)

ABSTRACT To minimize the anticipated shocks to economic, environmental, and social systems for developing and least developed countries, the reduction of Greenhouse Gas (GHG) emissions is mandatory to a large extend. The nuclear-renewable integrated system is proficient in optimal energy distribution to multiple production schemes to reduce GHG emissions and maximize profit. This paper addresses the hybridization of the micronuclear reactor and Renewable Energy Sources (RESs) Energy Sources (RESs) to develop a flexible, cost-effective, sustainable, and resilient off-grid Hybrid Energy System (HES). The paper presents three types of hybridization methods, termed ''Direct Coupling,'' ''Single Resource and Multiple products-based Coupling,'' and ''Multiple Resources and Multiple products-based Coupling.'' The hybridization techniques are used to plan and identify the most efficient Nuclear-Renewable Micro-Hybrid Energy System (N-R MHES). The sizing, performance, and characterization of N-R MHES solely depend on the RES and load characteristics' availability. Based on proposed hybridization techniques, mathematical modeling of N-R MHES's economy is carried out in the MATLAB environment. An artificial intelligence optimization algorithm, namely Particle Swarm Optimization (PSO), is used to minimize the Net Present Cost (NPC) and achieve the optimal system configurations of different N-R MHESs. The simulation results determine that ''Multiple Resources and Multiple Products-based N-R MHES'' provides around 1.8 times and 1.3 times lower NPC than ''Single Resource and Multiple products-based Coupling'' and ''Multiple Resources and Multiple products-based Coupling,'' respectively, with an acceptable margin of reliability. A sensitivity analysis has also been conducted in this paper to strengthen the findings of the study.

INDEX TERMS Micro-scale nuclear power generation, nuclear-renewable hybridization, renewable energy sources, sensitivity analysis.

I. NOMENCLATURE

A. ACRONYMS

BES	Battery Energy Storage
BG	Biogas Generator
CHP	Combined Heat and Power
COE	Cost of Energy
E2H unit	Electricity-to-Heat conversion unit
FC	Fuel Cell
GRF	Generation Reliability Factor
HES	Hybrid Energy System
H2E unit	Heat-to-Electricity conversion unit
KPI	Key Performance Indicator
LA	Level of Autonomy
LPSP	Loss of Power Supply Probability
MEG	Micro Energy Grid
MMR	Micro Modular Reactor
NPC	Net Present Cost
N-R HES	Nuclear-Renewable Hybrid Energy System
N-R MHES	Nuclear-Renewable Micro-Hybrid Energy System
O&M	Operations and Maintenance
PSO	Particle Swarm Optimization
PV	Photovoltaic
RES	Renewable Energy Source

The associate editor coordinating the review of this manuscript and approving it for publication was Zhuang Xu.

SEF	Surplus Energy Fraction
SOC	State of Charge
TES	Thermal Energy Storage
UOIT	University of Ontario Institute of Technology
WT	Wind Turbine

B. VARIABLES AND PARAMETERS

BES^{y}_{SOC} (t)	SOC of BES at time step t in year y (%).
BES^{max}_{cap}	Maximum capacity limit of BES (kWh).
C^{i}_{cap}	Capital cost ($).
C^{i}_{rep}	Present worth of replacement cost ($).
$C^{i}_{O\&M}$	Present worth of O&M cost ($).
C^{i}_{fuel}	Present worth of fuel cost ($).
C^{i}_{salv}	Salvage value ($).
C^{MMR}_{dec}	Present worth of MMR decommissioning cost ($).
C^{MMR}_{refuel}	Present worth of MMR refueling cost ($).
$C^{unit(i)}_{cap}$	Capital cost per equipment ($).
$C^{MMR(1st)}_{cap}$	Capital cost of 1st MMR unit ($).
$C^{unit(i)}_{rep}$	Replacement cost per component ($).
ceil(Y)	Function rounding the element Y to the closest integer that is greater or equal than Y.
$C^{annual(i)}_{O\&M}$	Annual O&M cost of a component ($/year).
$C^{annual(i)}_{fuel}$	Annual fuel cost of MMR ($/year).
$C^{MMR(annual)}_{dec}$	MMR decommissioning cost accrued per year ($/year).
$C^{MMR(unit)}_{refuel}$	Refueling cost of MMR fuel module ($).
η^{MMR}_{CHP}	Required CHP efficiency of MMR (%).
$\eta^{MMR(max)}_{CHP}$	Maximum CHP efficiency of MMR (%).
f	Inflation rate (%).
G	Set of system components.
$Htank^{y}_{SOC}$(t)	SOC of hydrogen tank at time t in year y (%).
$Htank^{min}_{SOC}$	Minimum SOC of hydrogen tank (%).
$Htank^{max}_{SOC}$	Maximum SOC of hydrogen tank (%).
HT_{cap}	Required capacity of hydro plant (kW).
HT^{max}_{cap}	Maximum capacity of hydro plant (kW).
i	An element of set G.
i′	Nominal discount rate (%).
$LPSP^{max}_{e}$	Maximum limit of electric LPSP (%).
$LPSP^{max}_{t}$	Maximum limit of thermal LPSP (%).
LT^{i}_{com}	Component lifespan (year).
LT^{i}_{rep}	Duration of replacement cost (year).
$LT^{rem}_{com(i)}$	Remaining lifetime of a component after project lifespan (year).
LT^{MMR}_{fule}	Lifespan of MMR fuel module (year).
N^{i}_{com}	Number of equipment.
N_{MMR}	Number of MMR unit.
N_{rep}	Number of replacements occurred for equipment.
N_{refuel}	Number of MMR refueling required.
N_{PV}	Number of PV panel.
N_{WT}	Number of WT.
N^{max}_{PV}	Maximum limit of the PV panel.
N^{max}_{WT}	Maximum limit of WT.
N^{max}_{MMR}	Maximum limit of MMR.
N^{max}_{Htank}	Maximum limit of hydrogen tank.
P^{i}_{gen}(t)	Electricity generation of a component at time t (kW).
$P^{i}_{gen,max}$	Maximum electricity generation of a component (kW).
P^{y}_{gen}(t)	Electricity generation at time t in year y (kW).
P^{y}_{EL} (t)	Electricity demand at time t in year y (kW).
P^{y}_{TL} (t)	Thermal demand at time t in year y (kW).
P_{PV} (t)	Generation by PV panel at time t (kW).
P_{W} (t)	Generation by WT at time t (kW).
P_{MMR} (t)	Electricity generation by MMR at time t (kW).
P_{HT} (t)	Generation by hydro plant at time t (kW).
P_{BG} (t)	Electricity generation by BG at time t (kW).
r	Real discount rate (%).
SEF^{max}_{e}	Maximum limit of electric SEF (%).
SEF^{max}_{t}	Maximum limit of thermal SEF (%).
T	Total simulation time
T_{PL}	Project lifespan (year).
T^{i}_{gen}(t)	Thermal power generation of a component at time t (kW).
$T^{i}_{gen,max}$	Maximum thermal power generation of a component at time t (kW).
T^{y}_{gen}(t)	Thermal power generation at time t in year y (kW).
T_{MMR} (t)	Thermal power generation by MMR at time t (kW).
T_{BG} (t)	Thermal power generation by BG at time t (kW).
TES^{y}_{SOC} (t)	SOC of TES at time t in year y (%).
TES^{max}_{cap}	Maximum capacity limit of TES (kWh).

II. INTRODUCTION

A. BACKGROUND AND MOTIVATION

The energy crisis leads to most of the challenges and opportunities that the world is facing nowadays. All energy production sources have shortcomings, such as air pollution, accidents, and Greenhouse Gas (GHG) emissions. About five

million premature death has been occurred every year due to air pollution [1]. Fossil fuel is the main contributor to air pollution. The energy generation accidents include mining of fossil fuel and uranium, raw material transportation, construction, oil, and gas extraction, and deployment. Though there are numerous downsides in energy generation, it varies significantly depending on the generation sources. Clearly, fossil fuel is the deadliest and dirtiest form of energy production source, whereas nuclear and Renewable Energy Source (RES)-based generation is the cleanest and safest one [2].

RESs-based Hybrid Energy System (HES) has been identified as a potential clean energy system to lessen GHG emissions. It also meets the growing electricity demand. However, due to variability, uncertainly, and a lower capacity factor of the RESs, it is quite challenging to achieve a 100% RES-based energy system. The flexibility measures, such as energy storage, can respond to the intermittency of RES in this type of scenario [3]. Stand-alone RES-based HES, combined with energy storage, is possible to some extent to serve small-scale energy demand. However, the sizing of energy storage, e.g., electric battery, Pumped Hydro Storage (PHS), and hydrogen, is critical for a microgrid. Large-scale PHS is available, but PHS is site-specific and has a high capital cost [4]. Hydrogen can be a possible massive energy storage media. Fuel Cell (FC) utilizes the stored hydrogen to generate electricity. Nonetheless, FC's efficiency is low (around 30%-60%) [5]. It is recommended to allow high penetration of renewables and install energy storage systems to overcome the drawbacks of intermittency. Therefore, the energy storage system is always indispensable, but a clean and continuous form of energy source is also required to minimize the vast energy storage requirement.

Because of the high fixed cost, high capacity factor, and base-load supply capability of Micro Modular Reactor (MMR), the stand-alone off-grid MMR-based energy system does not provide flexible and economic operation [6]. A vast amount of energy will be wasted in this type of off-grid energy system even if the energy storage is included. The stand-alone off-grid MMR-based energy system also elongates the energy storage sizing unnecessary since the surplus energy cannot be sold to the electric grid [7]. Hence, energy-mix is an essential pathway for the global energy crisis solution. The optimal range of contribution of renewable, nuclear, and gas technology in a hybrid system should be 50%, 50-60%, and 70-80%, respectively [8]. However, gas technology produces a significant amount of GHG emissions.

Different manufacturers are planning several types of power supply facilities, such as mobile microgrid powered by RESs and portable energy storage systems, for off-grid application. These facilities need extensive energy storage systems, fuel storage, and diesel generator for continuous power supply. It might be a suitable solution for a small community with minimal energy demand [9]. Still, a traditional microgrid is not competent in handling large scale commercial and industrial loads in a remote area. Therefore, a small-scale nuclear reactor integrated with RES could be a possible solution for medium/large-scale energy demand in a far-off location.

B. LITERATURE REVIEW

Bragg-Sitton *et al.* (2014) have defined a nuclear-renewable hybrid system as an energy network that fundamentally accomplishes the grid electricity demand and drives an additional industrial product generation process by surplus thermal or electric energy [10]. The secondary industrial process may include upgradation of synthetic fuel by heating, desalinated water production by electricity and heat, titanium dioxide production by thermal energy, district heating, and productions in paper mills [11]. Ruth and Cutler (2017) defined the Nuclear-Renewable Hybrid Energy System (N-R HES) as a single energy generation interface consisting of a nuclear reactor, at least one renewable resource, and an industrial process that utilizes electric or thermal energy, or both [12].

Ruth *et al.* (2014) listed six interconnection process of nuclear-renewable integration: thermal, electrical, chemical, mechanical, hydrogen, and information [13]. A detailed research and development plan on dynamic modeling, simulation, component development, and experimentation of the N-R HES has been presented in [14]. It has offered a valuable framework to analyze the N-R HES. The N-R HES has been classified into three types: tightly coupled N-R HES, thermally coupled N-R HES, and loosely coupled N-R HES. It is expected to proceed physically available N-R HES infrastructure by 2030.

Sabharwall *et al.* (2015) carried out an economic analysis of three different nuclear-renewable integration cases. A sensitivity analysis was also conducted in the study. The result showed that the nuclear reactor, combined with wind and hydrogen systems, had the economic potential [15].

A grid-connected N-R HES was assessed in [16] with a flexible load, named high-temperature steam electrolysis (HTSE). The research primarily concentrated on the modeling and control of the system equipment in Modelica. The study claimed reliable steady-state operation of Nuclear Power Plant (NPP), high-penetration of RES with resiliency, and efficient production of alternative commodities, such as oxygen and hydrogen. Since a Light Water Reactor (LWR) was used in this study, and the HTSE required high input temperature, it was suggested to include temperature-boosting technology with the HTSE system. Furthermore, the investigation asserted grid stability by satisfying demand and system constraints.

Garcia *et al.* (2016) configured Nuclear Hybrid Energy System (NHES) with multiple commodities productions and grid stability. NHES model was also capable of planning uncertainly, Key Performance Indicator (KPI) optimization, and real-time energy management. NHES was superior to conventional energy systems in terms of identifying uncertainly and high-level penetration of RES. Besides, NHES can reduce GHG emissions significantly by serving the grid and industrial demand with baseload heat generators, i.e., nuclear

reactors and RESs. However, the simulation carried out by Garcia *et al.* was not verified with real data obtained from industries. The probabilistic modeling and uncertainly of the sources were also overlooked in the study [17].

Mag *et al.* (2016) investigated the concept of the hybrid nuclear plant where a Small Modular Reactor (SMR) and solar photovoltaic (PV) were considered. This hybrid plant also consisted of molten salt Thermal Energy Storage (TES) system. Electricity from photovoltaic was converted into heat and used for the superheating of nuclear steam. The investigation determined that the hybrid nuclear power plant was more efficient than the standalone NPP. The molten salt storage served as extensive and indirect energy storage. The authors proved that thermal storage was more cost-effective than compressed air storage and competitive with pumped hydro storage, in terms of capital cost and round-trip efficiency. The study also concluded that the hybrid NPP has a lower initial cost per kilowatt than the standalone NPP. However, the nuclear reactor considered in this research was not commercially available [18].

Epiney *et al.* (2020) stated the necessity of installing a large-scale flexible generator, such as gas turbines, for absorbing electricity demand fluctuation that can be reduced by the concept of N-R HES. A RAVEN/Modelica-based software framework was demonstrated here to appraise the economic aspects of N-R HES. The research asserted that financial profits could be attained by incorporating the proper industrial process into the nuclear reactor. The study also examined a general case for implementing the proposed framework. Nevertheless, the methodology needs to be validated by real data, such as wind speed and industrial load demand, that are dependent on geographical conditions [19].

Chen *et al.* (2016) optimized two configurations of NHESs to understand system complexity, difficulties, and opportunities at the location of Texas and Arizona, USA. The generation plant consisted of an SMR, wind energy, PV, and electric grid. The additional energy conversion units produced chemical products, such as gasoline, Liquefied Petroleum Gas (LPG), and freshwater. The research demonstrated that the proposed optimizer could achieve economic gain. The study also supported the view that higher profit can be achieved if the system decreases its' participation to produce electricity and increases its' participation to produce alternative commodities like gasoline, freshwater, and LPG. The research recommended that online optimization should be developed to work with real-time commodity prices and the energy market [20].

Gabbar *et al.* (2020) revealed and compared five different cases, such as traditional fossil fuel-based energy system, fossil fuel/RES-based HES, standalone RES-based energy system, standalone nuclear energy system, and Nuclear-Renewable Micro-Hybrid Energy System (N-R MHES). Small-scale N-R HES could be an excellent option of continuous electricity supply for off-grid applications in terms of the discount rate, inflation rate, and project lifetime. N-R MHES provided the best resiliency and reliability to the demand for long term energy policy. Besides, modular N-R HES has the potential to reduce the amount of GHG significantly [7].

Progress on the development of N-R HES was exhibited in [21] by modeling a small scale reactor in Modelica software. The demonstration showed the design simplicity of reactor design and simple module alteration in Modelica. However, the model focused more on the features of Modelica software than the development and integration of the complete N-R HES. Recently, the International Atomic Energy Agency (IAEA) has issued a report on nuclear-renewable integration [22]. The report has comprised several case studies, prospects, applications of N-R HES, opportunities and challenges of nuclear-renewable integration, and the small-scale reactors' role in nuclear-renewable integration. The document also discussed the nuclear and energy policy of different counties to accelerate the innovation of nuclear-renewable integration.

Epiney *et al.* (2018) described a case study on the installation of a Reverse Osmosis (RO) plant for water supply, collaborated with Arizona Public Supply (APS). The study mainly focused on applying N-R HES software framework to conduct the case, as mentioned above. Three different cases were developed and analyzed in this study. A sensitivity analysis was carried out at the end of the investigation by varying different system parameters, such as discount rate, wholesale electricity price, project lifetime, net demand projection, and amount of salty water. However, N-R HES modeling was not presented in the study [23]. A similar case study has been conducted by Kim and Garcia (2015) in [24]. They also proposed a nuclear/PV HES for water desalination plants by the RO process. HES was modeled in an object-oriented Modelica interface. Moreover, the authors evaluated the system response due to step-change in variable electrical load and PV penetration. Technical issues were the main interests of this study.

Ruth *et al.* (2016) has analyzed two scenarios of N-R HES. The first scenario considered a nuclear reactor, thermal power cycle, Wind Turbine (WT), and synthetic gasoline production plant in Texas. The second scenario included a nuclear reactor, a PV panel, a thermal power cycle, and a desalination plant. The economy of N-R HES was compared with the available natural gas system for both scenarios. N-R HES of the study primarily focused on serving the industrial process. The research team found N-R HES as a potentially profitable candidate system compared to other technologies [25]. The authors extended this research in [12] by highlighting the economic potential of N-R HES for hydrogen production.

Redfoot and Borrelli (2018) indicated the similarities between the Nuclear Fuel Cycle Simulator (NFCS) and the required modeling features of N-R HES. The authors addressed the necessary functionalities of N-R HES and the already developed software used to model N-R HES. The required functionalities of an N-R HES included dynamic feature, component optimization, stochastic model of renewables, grid demand model, economic KPIs, and sensitivity

analysis. The authors recommend incorporating new components, flexibility, financial tools, open-source tool, physical modeling tools, and uncertainty tools into NFCS in the future to get benefits in N-R HES modeling [26].

C. CONTRIBUTION

The paper mainly concentrates on micro-scale nuclear-renewable integration techniques for off-grid applications. This paper aims to evaluate the proposed nuclear-renewable hybridization methods and identify the most-effective coupling techniques. Detailed modeling and analysis have been carried out to determine the best hybridization method for micro-level nuclear-renewable integration.

Three different coupling methods for nuclear-renewable integration are introduced in this study. The hybridization procedures, along with energy management algorithms, are implemented in the MATLAB environment. Though the previous works on the large/small-scale nuclear-renewable integrated system are carried on the physical component-based simulator, such as Modelica and RAVEN, this study is conducted in the most versatile and popular simulator, MATLAB. No research is found on mathematical modeling and comparison for N-R MHES hybridization techniques.

A metaheuristic optimization algorithm, Particle Swarm Optimization (PSO), is developed and executed in the proposed system arrangement to identify the system's best configuration. System reliability constraints are efficiently utilized in the optimization constraints, rather than using them as an objective function. It reduces optimization complexity.

Since the demand varies from region to region and availability of RESs are highly dependent on the meteorological condition, a sensitivity analysis is carried out widely to determine the system parameters' effect on planning, economy, and resiliency. The sensitivity analysis ensures that the results obtained in the base cases are not confined for a particular project location or specific load demand; the research findings are valid regardless of the load demand and project site. The sensitivity analysis also provides ample information to the system planners regarding the impact of different system equipment on system economy and resiliency. It will help in the deployment stage in the future

III. HYBRIDIZATION METHODS OF NUCLEAR-RENEWABLE MICRO-HYBRID ENERGY SYSTEM (N-R MHES)

Micro Energy Grid (MEG) is an integrated energy system that concurrently supplies electric and heat energy [27]. MEG, along with microreactors, is termed as "N-R MHES." N-R MHES is a combination of a very small-scale nuclear reactor, called MMR, and different RESs. N-R MHES provides a resilient energy supply for electric and thermal demand for off-grid applications. The Distributed Generation (DG) principle is also implemented in N-R MHES. Combined Heat and Power (CHP) criteria are often applied in N-R MHES, but there are no binding rules for CHP implementation. An N-R MHES provides virtually zero carbon footprint since no fossil fuel is burnt within the system. However, some GHGs are released at mining, construction phase of the system, fuel and raw materials shipment, decommissioning, and waste management [28].

Based on resource arrangement, three types of hybridization techniques of N-R MHES for off-grid applications are proposed in this paper. The detailed system architecture is discussed as follows.

A. DIRECT COUPLING

In direct coupling technique, electricity production is the primary concern within the HES. The hybrid system incorporates all available energy generation sources, such as nuclear reactor, wind power, hydropower, solar power, biogas (biofuel), and geothermal power, depending on the topographical characteristics. The generation sources produce electricity individually and combine at a common coupling point. CHP facility and by-product commodities are not viewed in this configuration. Hence, thermal generation is not available in this infrastructure. As there is no direct thermal generation with HES, the schematic does not include any TES. Electrochemical, chemical, electrical, and mechanical energy storage systems might be added to store the excess electricity. Fig. 1 depicts a system schematic of directly coupled N-R MHES.

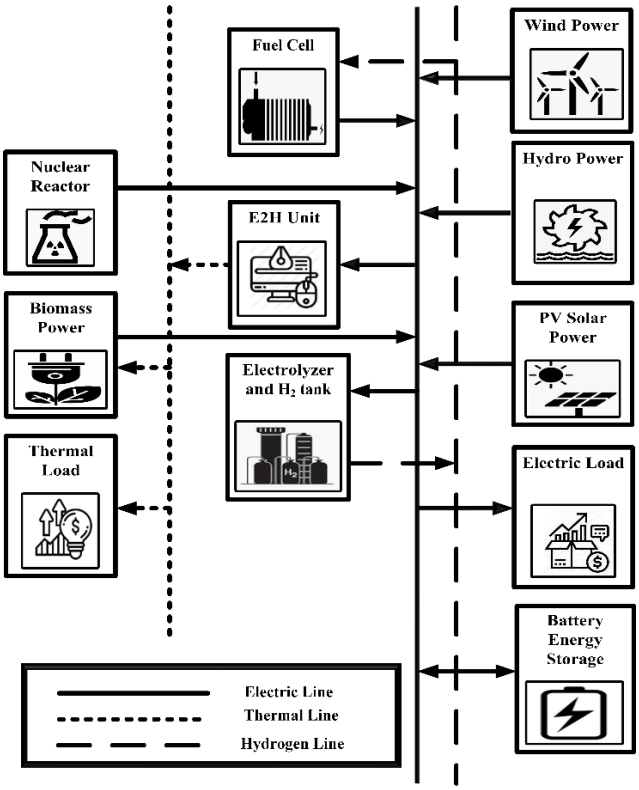

FIGURE 1. Grid-level coupled system.

One of the conventional renewable sources, geothermal energy, is not added in Fig. 1 since geothermal energy depends on geographical conditions. For the same reason, pumped hydro energy storage is not considered in this paper.

In directly coupled N-R MHES, the electric requirement is fulfilled by direct electricity generation. On the other hand, the thermal demand is met by the Electricity-to-Heat conversion(E2H) unit. E2H unit converts electric energy into thermal energy. The N-R MHES supplies the required thermal power to the biogas production plant for all types of hybridization techniques presented in this paper.

In the energy management algorithm, a hierarchy is maintained in the charging and discharging of the storage. Hydrogen storage is introduced in the proposed HES to reduce Battery Energy Storage (BES) sizing. Hydrogen storage has a higher priority than BES in the charging and discharging mechanism. If there is any surplus electricity available, it will be stored in the hydrogen tank, followed by the BES. Similarly, the shortage of electric and thermal demand will be fulfilled by FC, followed by the BES. FC utilizes the stored hydrogen to generate electricity. After charging the hydrogen tank and BES, if there is any excess electric energy available, it will be consumed by electrical dump loads.

Any sort of combination by renewables, energy storages, and loads are plausible within this type of N-R MHES. The arrangement of different equipment is not limited to the proposed N-R MHES shown in this paper. However, the fundamentals of energy management must be maintained in extended or reduced types directly coupled N-R MHES.

B. SINGLE RESOURCE AND MULTIPLE PRODUCTS-BASED COUPLING

In this coupling, the single generation source is a nuclear reactor that will provide thermal and electrical energy. Biogas Generator (BG) can be combined with this type of coupling since the required thermal energy for the biogas plant comes from either the nuclear reactor or the biogas plant or both. The conventional RESs are not viewed within this kind of hybridization. Fig. 2 shows the detailed architecture of a single resource and multiple products-based coupling. The generated electrical power from the nuclear reactor and BG directly serves the electric load. The recovered waste thermal energy from the nuclear reactor and BG is utilized to serve thermal demand and different thermal applications. For instance, a part of electricity and waste heat can be utilized in the seawater desalination plant and hydrogen production plant. In this type of coupling, the secondary byproduct, such as hydrogen and biofuel, is counted as resources for generating electricity or other products. Since electrical and thermal generators are available within HES, this system configuration can combine electric, electrochemical, thermal, and mechanical energy storage systems. The Heat-to-Electricity (H2E) unit and E2H unit are inserted to ensure the ultimate reliability of energy supply. However, the H2E unit and the E2H unit will have the least preference and will be operated in extreme cases.

In electrical energy management, the excess electric energy will be stored in hydrogen storage after fulfilling the electric demand, followed by BES. The further excess electricity will

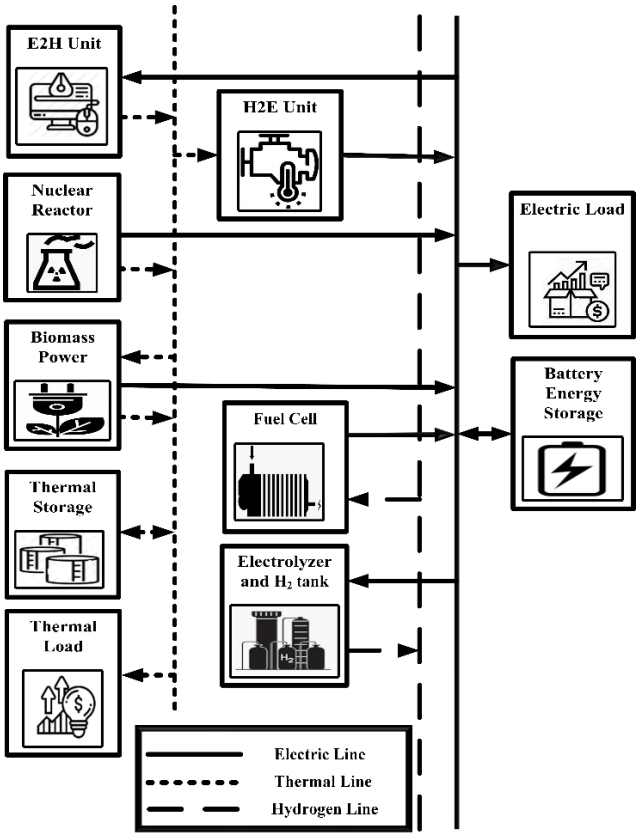

FIGURE 2. Single resource and multiple products-based coupled system.

be utilized to serve the thermal demand, if needed, through the E2H unit. The rest of the available surplus electric energy will be consumed by the electric dump load. Similarly, hydrogen storage will discharge first to accomplish electric demand shortage, followed by BES. The H2E unit will only operate if hydrogen storage and BES are unable to fulfill the electric demand.

In thermal energy management, TES will store the excess thermal energy. The additional surplus thermal energy can be used to serve the electric demand by the H2E unit if required. The thermal dump load will consume the rest of the available excess thermal energy. Likewise, TES will discharge to satisfy the deficit thermal demand. The E2H unit will operate to meet the further thermal energy shortage. Both H2E and E2H have the least precedence in the energy management algorithm.

C. MULTIPLE RESOURCES AND MULTIPLE PRODUCTS-BASED COUPLING

Multiple Resources and Multiple Products-based coupling is a blended hybridization technique of ''direct coupling'' and ''single resource and multiple products-based coupling.'' It offers multi-level coupling, e.g., electrical and thermal, to produce all possible commodities. In this type of system, MMR, PV panel, WT, BG, and hydro plant serve the electric demand. Conversely, the recovered waste heat from MMR

and BG fulfill the thermal demand. The energy management algorithm and all the system components' functionalities for this coupling technique are identical to the single resource and multiple products-based coupling. Secondary commodities and CHP principle are also regarded in this hybridization method. All the traditional renewables can be considered in this system, whereas only BG is viewed as the only renewable source in the single resource and multiple products-based coupling. Fig. 3 represents the system configuration of the multiple resources and multiple products-based coupled system.

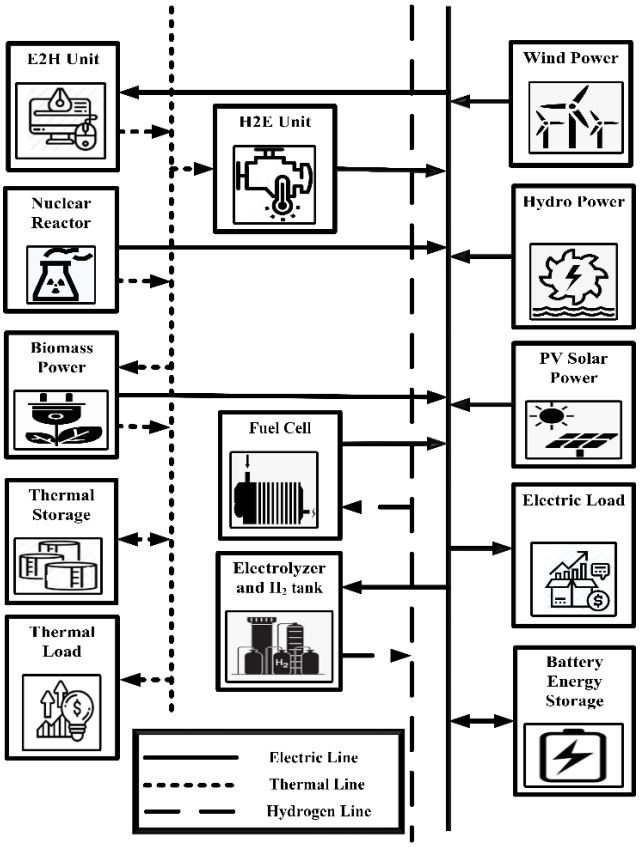

FIGURE 3. Multiple resources and multiple products-based coupled system.

IV. SYSTEM MODELING

The proposed nuclear-renewable integration techniques are developed in MATLAB simulator. The required model for each of the system components is developed in MATLAB and the PSO algorithm is implemented to obtain the optimal configuration. Since the study requires electric and thermal load demand for a location, Ontario Tech University (UOIT) campus is selected as the project location. The electric load data of the UOIT campus is collected for the study. Since the original thermal load profile for the UOIT campus is not available, a typical thermal load profile is captured from the HOMER Pro software library. Since electric demand is higher than thermal demand for most of the usual cases [29], the average thermal demand is as assumed lower than the electric demand.

Hourly data of system demand and resources for one year, a total of 8760 data (365 days $\times$ 24 hours/day) points, are used in the simulation. Each month is segmented as one window and represented by 24 data points to reduce the computational burden and simulation time. As daily demand variation within a month is insignificant, the daily system demand for each month is considered as same. But, the energy demand varies from month to month. It leads to utilizing 288 data (12 month $\times$ 1 day/month $\times$ 24 hours/day) points in the simulation rather than using 8760 data points [30]. The electric and the thermal load profiles in this study are presented in Fig. 4 and Fig. 5, respectively.

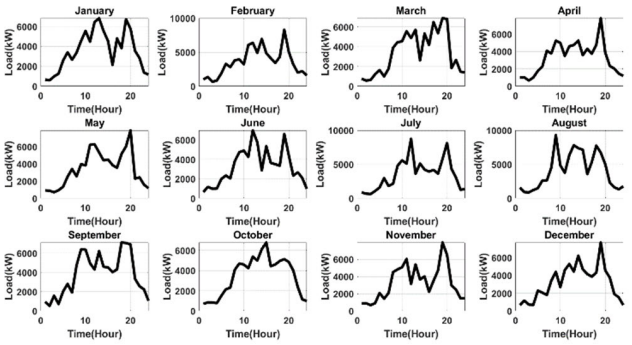

FIGURE 4. Electric demand.

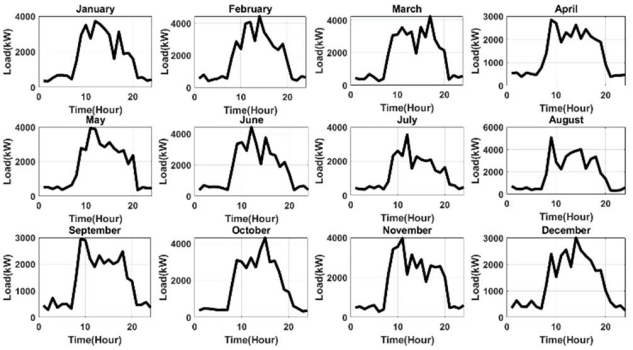

FIGURE 5. Thermal demand.

A. MICRO MODULAR REACTOR (MMR)

MMR is a fourth-generation micro-scale nuclear reactor that affords clean, reliable, and cost-efficient electric and thermal power. MMR is specially designed for remote residential and industrial applications where there is no footprint of the electric grid. It has a CHP provision that facilitates MMR to generate electrical and thermal energy simultaneously. It reduces electric and thermal power generation by up to 50%. Since MMR does not release any GHG emissions during operation, it reduces 100% carbon emissions. MMR is developed in industries and brought it as a package at the project location. It requires a small size of concrete foundation. The reactor is sized concerning the international standard of portable containers so that the reactor can be exported to any license

location by ship, rail, or road. The reactor is sealed and does not require to refuel at its lifetime. Thus, it assures the utmost security of fuel supply. The fuel module is discharged from MMR facility at the end of its lifetime and kept in a commissioned nuclear waste management facility. A new fuel module replaces the old module; no engineering work is done with the fuel module at the site. No spent fuel facility is located at the reactor site. Hence, MMR's design provides excellent environmental protection. The development cost of MMR is also lower compared to SMR and other fourth-generation nuclear reactors. Since a large portion of MMR financing is associated with sunk cost, the energy cost and economic risks are entirely predictable for MMR [31].

The paper mainly focuses on the economic model of MMR. The discussion on the licensing processes, security, and the regulation procedure is beyond this study. MMR installation cost depends on numerous factors, e.g., engineering technology, plant layout, environmental requirements, civil works, licensed area, financing plan, transportation facility, and employees. Transmission and Distribution (T&D) cost is usually incorporated with all kinds of technology. Thus, the T&D cost is ignored in this paper. The installation of MMR qualifies for the Production Tax Credits (PTCs). Although PTCs are mainly associated with renewable-based HES [32], PTCs are also available for nuclear energy up to 6000 MWe. But, PTC is not included in this MMR economic model due to the trivial impact of PTC on the MMR economy [33].

Usually, the cumulative production cost of a first-of-a-kind component decreases with gaining experiences. Thus, the installation cost of an MMR is higher than the next MMR unit deployment cost. The knowledge and the experience gained with time are termed as "learning rate." The relationship between cost reduction and the learning rate is expressed by the "one-factor learning curve" presented in (1) [34].

$$\mathrm{LR} = 1 - 2^{\mathrm{R}} \tag{1}$$

where LR is the learning rate (%), and R is the cost reduction rate (%).

Factory-manufactured MMR has a higher learning rate than the on-site assembled MMR. Besides, the learning rate will be higher in a dedicated MMR production factory than a mixed MMR production factory with other commodities. The overnight capital cost reduction of MMR exhibits different trends for different learning rates

Fig. 6 shows different scenarios of MMR capital cost reduction due to various learning rates. Capital cost reduction of MMR due to the learning rate is expressed by (2) [35].

$$\mathrm{C_u} = \mathrm{C_{1st}} \times \mathrm{N_{th}^R} \tag{2}$$

where $\mathrm{C_u}$ is the unit cost of MMR of $\mathrm{N_{th}}$ number MMR unit ($), and $\mathrm{C_{1st}}$ is the 1st MMR unit cost ($).

The input parameters of the MMR investigated in the paper are presented in Table 1 [33].

Typically, factory-assembled products experience a learning rate of 15-20% [36]. Since MMR is also a factory-made product, MMR's learning rate is expected to 5%-15%.

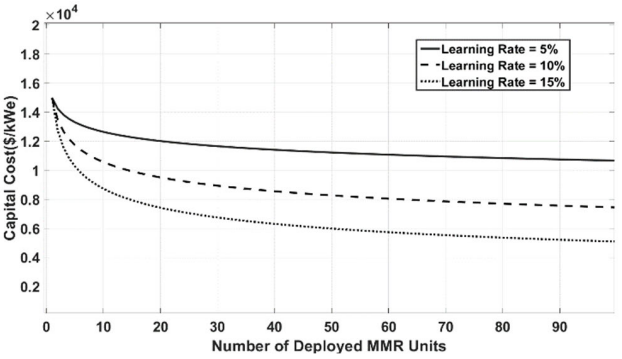

FIGURE 6. Capital cost reduction for different learning rates.

TABLE 1. Specification of the MMR unit.

Parameters	Value
Reactor size (kW_e)	1000
Plant Lifespan (Years)	40
Core Lifespan (Years)	10
Capacity Factor (%)	95
Overnight Capital Cost ($\$/kW_e$)	15,000
Fixed O&M Cost ($\$/kW_e$)	350
Fuel Cost ($\$/MWh$)	10
Decommissioning Cost ($\$/MWh$)	5
Fuel Module Refueling Cost ($)	20 million
Plant Efficiency (%)	40

Besides, the Korea Hydro and Nuclear Power has encountered a learning rate of 10%. As MMR is factory-manufactured equipment, a learning rate between 5% to 10% is expected for MMR [37]. In this paper, the learning rate for MMR production is considered as 10%. The Operations and Maintenance (O&M) cost and the fuel price are also expected to decrease with the lessons learned. But, these types of cost reductions are not considered in this paper due to the insignificant impact of O&M cost and fuel cost on the MMR economy model [38].

The MMR economic model consolidates MMR licensing cost and site engineering cost in the overnight capital cost. The inclusion of MMR refurbishment cost separately may not fit in MMR's economic model because of different operational strategies. Some may replace the entire nuclear reactor, refurbish it at the central facilities, refuel it, and then reuse it. On the other hand, some may only refuel the reactor in-place and not carry out any refurbishment. Hence, the refurbishment cost is combined into the fixed O&M cost in this paper rather than individually. The fuel management cost is added in the fuel cost, indicated in Table 1. The MMR decommissioning cost is evenly spread over the project lifespan and accumulated during the operation of MMR. The fuel module transportation cost and the installation cost at the licensed-site are incorporated in the refueling cost, mentioned in Table 1. As MMR fuel cost is captured in "Fuel Cost" indicated in Table 1, the refueling does not involve the MMR fuel cost.

Nuclear power plant operation is primarily categorized into two sections: baseload power plant and load-following power plant [39]. MMR-based NPP is also capable of operating in both modes. The baseload operation provides a constant power level at its nominal capacity. The baseload MMR is only unavailable during the maintenance or refurbishment period. On the contrary, the load-following procedure adjusts its output power depending on load variations. Though traditional large-scale reactors are not operated in load-following mode, the modern microreactor has the capability of load-following operation. Load-following of microreactors is achieved by adjusting the reactor control rods, bypassing steam turbines, and making one or multiple units offline [40].

Load-following MMR's operation is a complicated procedure. Load-following operation is also expected to face substantial thermo-mechanical stress. Besides, the load-following strategy affects the primary steam supply and reactor coolant systems, leading to frequent replacement of that equipment. The load-following technique also affects heat exchanger due to the rapid rate of temperature change. The small/micro-scale reactor can perform load-following from 100% to as low as 20% power. This kind of reactor's power ramp is linear, and it is around 5% per minute. Rates of power ramp and duration of low power operation are restricted with a defined limit. Another critical issue with load-following is fuel Pellet Cladding Interaction (PCI) at greater than 5% per minute power ramp. But lower reactor power density, like a micro-scale reactor, slightly reduces the risk [40]. Moreover, adjusting a baseload system, e.g., NPP, to manage variable system demand causes significant wear and tear on the structure and increases O&M cost [41].

The capital cost is the primary driver of MMR's total deployment cost. Besides, the MMR fuel cost and the O&M cost do not rely on the amount of energy production. The load-following operation reduces MMR's energy generation since it generates energy by following the demand profile. Therefore, load-following MMR is not cost-efficient. However, secondary commodities production by excess thermal generation utilizing CHP may lead to improve the investment economics [38]. Conversely, the base-load MMR operation is simple. For HES, the rest of the demand is met by dispatchable generation sources and variable RES along with energy storage systems. The appropriate energy mix depends on total system cost, availability, and optimal system configuration [42].

Moreover, load-following NPP is required if a significant portion of energy contribution comes from nuclear generation [43]. The energy mix of renewables with nuclear reduces the substantial contribution of nuclear generation in HES. By analyzing all the factors discussed above, MMR's baseload operation is regarded in this paper. Energy storage systems are also included to meet the variable system demand. The waste heat is recovered and utilized in cogeneration to produce useable thermal power.

B. SOLAR PV PANEL

PV panel output power can be determined by the following equations [44]. The Location of solar data is the UOIT campus.

$$T_c(t) = T_a(t) + \left(\frac{NCT - 20}{800}\right) \times G_t(t) \quad \forall t \in T \tag{3}$$

$$\eta_{PV}(t) = \eta_{ref} \times \eta_{MPPT} \times [1 + \alpha(T_c(t) - T_{cref})] \quad \forall t \in T \tag{4}$$

$$P_{pv}(t) = N_{PV} \times \eta_{PV}(t) \times PV_{area} \times G_t(t) \quad \forall t \in T \tag{5}$$

where $T_a(t)$ is the ambient temperature (°C), NCT is the nominal operating cell temperature (45 °C), $G_t(t)$ is the solar irradiance (kW/m^2), $\eta_{PV}(t)$ is the instantaneous efficiency of PV panel (%), η_{ref} is the PV panel reference efficiency (17.3 %), η_{MPPT} is the efficiency of the Maximum Power Point Tracking (MPPT) unit (95 %), α is the temperature coefficient (-0.41 °C^{-1}), T_{cref} is the PV panel reference temperature (25 °C), N_{PV} is the number of PV panel, and PV_{area} is the area occupied by a unit PV panel (5m^2).

A single year solar irradiance and temperature for the selected location are collected and shown in Fig. 7 and Fig. 8, respectively [45]. The capital cost, replacement cost, maintenance cost, and lifetime of a single PV panel are considered as 1200 $/kW [46], 1000 $/kW [46], 12 $/kW/year [47], and 25 years [48], respectively.

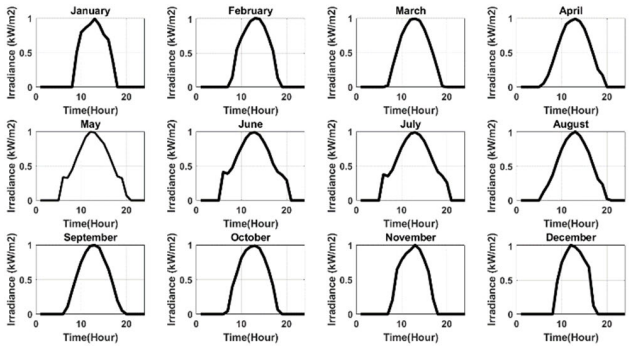

FIGURE 7. Solar irradiance.

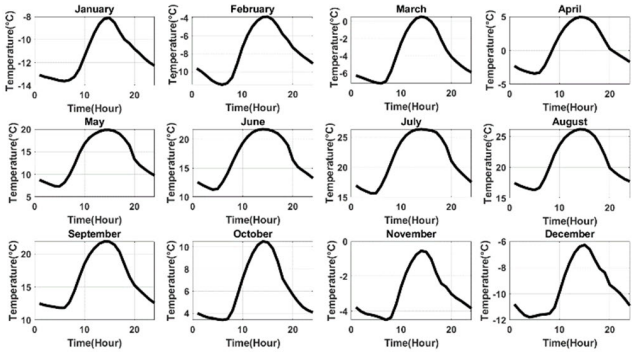

FIGURE 8. Temperature.

C. WIND TURBINE

To calculate wind power, firstly, wind speed for a particular location is calculated at the WT hub height. Equation (6) calculates the wind speed at the hub height [49].

$$V(t) = V_r(t) \times \left(\frac{h_{hub}}{h_r}\right)^a \quad \forall t \in T \tag{6}$$

where V(t) is the calculated wind speed (m/s), $V_r(t)$ is the wind speed at the anemometer height (m/s), h_{hub} is the hub height (16 m) [50], h_r is the anemometer height (50 m) [45], and a is the power-law exponent (1/7) [49].

The actual wind power generation from WT is determined by (7).

$$P_w(t) = \begin{cases} 0, & V(t) < V_{min}, V(t) > V_{max} \\ AP_r & V_{min} \le V(t) \le V_r(t) \\ P_r, & V_r \le V(t) \le V_{max} \end{cases}$$
$$A = \frac{V^3}{V_r^3 - V_{min}^3} - \frac{V_{min}^3}{V_r^3 - V_{min}^3} \tag{7}$$

where P_r is the WT rated power (10 kW), V_r is the rated wind speed (6 m/s), V_{min} is the minimum wind speed (2.75 m/s), and V_{max} is the maximum wind speed (20 m/s) [50].

The wind speed data for the project location are represented in Fig. 9 [45]. The initial cost, replacement cost, maintenance cost, and lifetime of the unit WT are 1130 $/kW [46], 1130 $/kW [46], 48 $/kW/year [51], and 25 years [52], respectively.

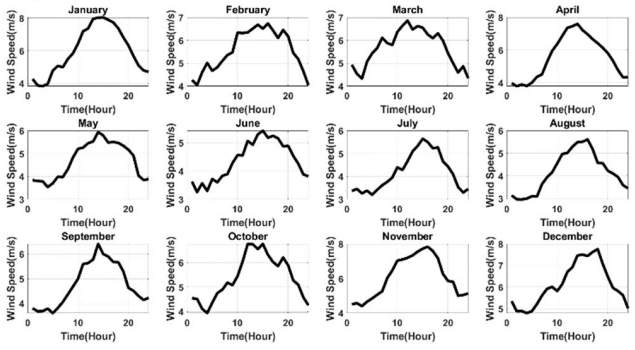

FIGURE 9. Wind speed.

D. HYDRO TURBINE

The run-of-river hydroelectric generation is considered in this study. Typically, the run-of-river hydropower plant provides a constant power supply [53]. The flow rate data of Lake Ontario, presented in Fig. 10, are obtained to calculate the hydro turbine power output [54]. Though there is a slight variation in daily streamflow, it is not significant. Thus, the interpretation is not prominently visible. The hydropower output is estimated by the following equations [55].

$$H_{eff} = H_a(1 - H_{loss}) \tag{8}$$
$$P_h(t) = H_{eff} \times \rho_w \times g \times Q_t(t) \times \eta_t \quad \forall t \in T \tag{9}$$

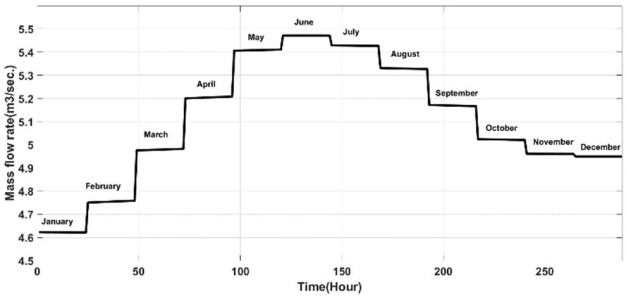

FIGURE 10. Streamflow.

where H_{eff}, H_a, H_{loss}, ρ_w, g, $Q_t(t)$, and η_t represent effective water head (m), available water head (25 m), head loss of pipe (15 %) [56], density of water (1000 kg/m^3), gravitational constant (9.8 m/s^2), water flow rate (m^3/s), and turbine efficiency (80 %) [57], respectively.

Again, the streamflow rate in the hydro turbine is utilized by (10).

$$Q_t(t) = \begin{cases} 0, & Q_a < Q_{min} \\ Q_a, & Q_{min} \le Q_a \le Q_{max} \\ Q_{max}, & Q_a > Q_{max} \end{cases} \tag{10}$$

where Q_a, Q_{min}, and Q_{max} denote available streamflow rate to hydro turbine (m^3/s), minimum stream flow rate to hydro turbine (50% of the flow rate), and maximum streamflow rate to hydro turbine (150% of the flow rate), respectively. The capital cost, replacement cost, maintenance cost, and lifespan of the hydro plant are 2500 $/kW, 250 $/kW, 100 $/kW/year, and 40 years, respectively [58]. The nominal capacity and the design flow rate of the hydroelectric plant are 1000.64 kW and 5.1 m^3/s, sequentially.

E. BIOGAS GENERATOR (BG)

Biogas is typically generated in Anaerobic Digestion (AD) process. In the AD process, digester is produced as a by-product along with biogas. A small-scale biogas plant having a rated capacity of 65.10 kW is regarded in this study. The biogas is produced from cow manure. The number of cows for the dairy farm is 150. The BG operates from 7.00 pm to 7.00 am since solar irradiance goes to zero in this time window; this compensates the solar PV panels availability at some extend within the HES. Equation (11) calculates the total biogas production in a year.

$$V_{BG} = N_a \times m_a \times k_{DS} \times k_{OS} \times v_B \times 365 \tag{11}$$

where V_{BG}, N_a, m_a, k_{DS}, k_{OS}, and v_B are the biogas production (m^3/year), number of animals in a particular group, manure produced per animal (37 kg/day) [59], dry substance content in the manure of a particular animal (0.23) [60], organic substance content in dry substance (0.85) [60], and specific biogas generated from the organic substance (0.3m^3/kg) [60], respectively.

The energy produced from biogas can be calculated by (12). This generated energy is the input of the CHP unit.

$$E_{bio} = V_{BG} \times e_B \tag{12}$$

where E_{bio} is the energy produced from biogas (kWh/year), and e_B is the specific heat energy of manure (6 kWh/m^3) [61].

Equation (13-14) calculate the generated electric and thermal power within the biogas plant, respectively.

$$P_{bio}(t) = \frac{E_{bio} \times \eta_{l,e}}{T_{oh}} \quad \forall t \in T \tag{13}$$

$$T_{bio}(t) = \frac{E_{bio} \times \eta_{l,t}}{T_{oh}} \quad \forall t \in T \tag{14}$$

where $\eta_{l,e}$ and $\eta_{l,t}$ are the electric (40%) and thermal (30%) efficiency of the CHP unit, sequentially [62], and T_{oh} is the number of operating hours in a year (4380 hours/year).

The required thermal energy to rise and maintain the digester temperature comes from HES. Equation (15) determines the amount of the necessary thermal energy. A 30% extra energy is added in (15) by regarding the losses [63].

$$Q_t = M \times s_f \times (T_d - T_f) \times 1.3 \tag{15}$$

where Q_t, M, s_f, T_d, T_f are the thermal energy required to heat the substrate material (kJ/year), combined manure and water flow rate (kg/year), specific heat capacity of substrate/feed (kJ.kg^{-1}.°C^{-1}) [64], temperature required in the digester (°C), and substrate/feed temperature (°C), respectively. As a rule of thumb, the specific heat of the substrate is the value of water (4.18 kJ.kg^{-1}.°C^{-1}). The slurry is pumped and kept in the digester at 35 °C [65]. The minimum substrate/feed temperature signifies the maximum heat energy consumption in the digester. Thus, 0°C is assumed as the substrate/feed temperature in this study, which could be the lowest substrate/feed temperature. The capital cost, replacement cost, O&M cost, and lifespan of the BG are 4000 $/kW, 2500 $/kW, 300 $/kW/Year, and 25 years, respectively [66].

F. FUEL CELL (FC), ELECTROLYZER, AND HYDROGEN STORAGE

FC, electrolyzer, and hydrogen tank are combined to store the surplus electricity in the form of hydrogen. Excess electricity is taken by electrolyzer that produces hydrogen from electricity. This hydrogen is stored in the hydrogen tank. The nominal capacity, capital cost, replacement cost, O&M cost, and lifespan of the hydrogen tank are 25 kg, 1200 $/kg, 800 $/kg, 15 $/kg/Year, and 25 years, respectively [67]. The stored hydrogen is used later to generate electricity by FC. Equation (16) is used to calculate the hydrogen production by electrolyzer [68], [69].

$$H_{pr}(t) = \frac{\eta_{ele} \times E_{ele}(t) \times D_H}{HV_H} \quad \forall t \in T \tag{16}$$

where η_{ele} is the electrolyzer efficiency (80 %) [70], $E_{ele}(t)$ is the input energy to the electrolyzer (kWh), D_H is the density of hydrogen (0.09 kg/m^3), and HV_H is the heating value of hydrogen in standard condition (3.4 kWh/m^3).

The energy generated by FC can be calculated by (17). The capital cost, replacement cost, O&M cost, and lifespan of the FC are 600 $/kW, 500 $/kW, 0.0153 $/kW, and 4.5 years, respectively [71].

$$E_{FC}(t) = \frac{[H_t(t-1) - H_t(t)] \times \eta_{l,FC} \times HV_H}{D_H} \quad \forall t \in T \tag{17}$$

where $\eta_{l,FC}$ is the FC efficiency (50%) [72], and $H_t(t)$ is the amount of hydrogen stored (kg) at time t.

G. BATTERY ENERGY STORAGE (BES)

Along with the hydrogen tank, the battery bank is also used within the system to store electric energy. The battery sizing (kWh) is estimated by (18) [73].

$$BES_{cap} = \frac{P_{EL}^{avg} \times AD \times N_{bat}}{DOD_{BES} \times \eta_{l,inv} \times \eta_{l,BES}} \tag{18}$$

where P_{EL}^{avg}, AD, N_{bat}, DOD_{BES}, $\eta_{l,inv}$, and $\eta_{l,BES}$ are the average electric load (kW), autonomy days (usually 3-5 days, 3 days are regarded here) [73], number of the battery unit, battery's depth of discharge (80 %), inverter efficiency (95 %) [74], and BES efficiency (85 %) [75], respectively.

The minimum and maximum State of Charge (SOC) of the BES are set by the following equations, respectively.

$$BES_{SOC}^{min} = BES_{cap} \times (1 - DOD_{BES}) \tag{19}$$

$$BES_{SOC}^{max} = BES_{cap} \times DOD_{BES} \tag{20}$$

The charging and discharging efficiency energy of BES at any time t can be described by (21) and (22), respectively.

$$E_{BES}(t) = E_{BES}(t-1) + E_{BES}^{in}(t)\eta_{l,BES} \quad \forall t \in T \tag{21}$$

$$E_{BES}(t) = E_{BES}(t-1) - \frac{E_{BES}^{out}(t)}{\eta_{l,BES}} \quad \forall t \in T \tag{22}$$

where $E_{BES}^{in}(t)$ is the possible BES charging energy (kWh), and $E_{BES}^{out}(t)$ is the available BES discharging energy (kWh). The initial cost, replacement cost, O&M cost, and lifetime of the BES are 398 $/kWh, 398 $/kWh, 10 $/kW/Year, and 5 years, respectively [71].

H. THERMAL ENERGY STORAGE (TES)

A generic hot and cold-water TES is adopted in this study. The minimum and maximum SOC of the TES are presented as follows. The capital cost, replacement cost, and lifespan of the TES are 5 $/kWh [76], 5 $/kWh [76], and 30 years [77], sequentially.

$$TES_{SOC}^{min} = TES_{cap} \times (1 - DOD_{TES}) \tag{23}$$

$$TES_{SOC}^{max} = TES_{cap} \times DOD_{TES} \tag{24}$$

where TES_{cap} is the TES capacity (kWh), and DOD_{TES} is the depth of discharge of the TES (80%).

The TES charging and discharging operation can be expressed by (25) and (26), respectively.

$$E_{TES}(t) = E_{TES}(t-1) + E^{in}_{TES}(t)\eta_{TES} \quad \forall t \in T \tag{25}$$

$$E_{TES}(t) = E_{TES}(t-1) - \frac{E^{out}_{TES}(t)}{\eta_{TES}} \quad \forall t \in T \tag{26}$$

where $E^{in}_{TES}(t)$ is the available input energy of the TES (kWh), $E^{out}_{TES}(t)$ is the discharging energy of the TES (kWh), and η_{TES} is the TES efficiency (80 %) [78].

I. ELECTRICITY-TO-HEAT (E2H) AND HEAT-TO-ELECTRICITY (H2E) UNIT

Both E2H and H2E units are introduced to ensure the utmost reliability of the HES. E2H unit and H2E unit operate in extreme cases when no other sources are available to serve electric or thermal demand.

Since, no other thermal generation is possible within the studied MEG to support thermal demand, the E2H unit utilizes the surplus electric energy to serve the thermal demand by converting electricity into thermal energy. The E2H unit is simply an electric boiler. The power generated by E2H is expressed by (27). The initial installation cost, replacement cost, and lifespan of the E2H are 54 $/kWh, 54 $/kWh, and 20 years [79], respectively.

$$E2H(t) = \eta_{E2H} \times T_{spls}(t) \quad \forall t \in T \tag{27}$$

where η_{E2H} is the H2E unit efficiency (98 %) [80], and $T_{spls}(t)$ is the excess electric power at time step t.

The H2E comprises of electric generators, steam generators, and steam turbines. The steam turbine requires high-pressure steam that is generated by the steam generator. The electric generator is coupled with the turbine, and eventually, electricity is generated from the electric generator. The capital cost, replacement cost, O&M cost, and lifetime of the H2E are 1932 $/kWh, 1932 $/kWh, 0.9 $/kW/Year, and 15 years [81], [82], sequentially. The power generated from an H2E unit by utilizing surplus thermal energy can be expressed by (28-29).

$$\eta_{H2E} = \eta_{EG} \times \eta_{ST} \times \eta_{SG} \tag{28}$$

$$H2E(t) = \eta_{H2E} \times P_{spls}(t) \quad \forall t \in T \tag{29}$$

where η_{EG}, η_{ST}, η_{SG}, and $P_{excess}(t)$ are the electric generator efficiency (95 %) [83], steam turbine efficiency (40 %) [84], steam generator efficiency (40 %) [85], and surplus thermal power at time t, respectively.

V. KEY PERFORMANCE INDICATORS (KPIs)

The following technical and economic KPIs are regarded in this study.

A. GENERATION RELIABILITY FACTOR (GRF)

GRF defines the percentage of system demand that is accomplished by the HES. Equation (30-31) present the mathematical expression of GRF for the electric and thermal load.

$$GRF_e = \frac{\sum_{t=1}^{T} P_{gen}(t) \times \Delta t}{\sum_{t=1}^{T} P_{EL}(t) \times \Delta t} \times 100\% \quad \forall t \in T \tag{30}$$

$$GRF_t = \frac{\sum_{t=1}^{T} T_{gen}(t) \times \Delta t}{\sum_{t=1}^{T} P_{TL}(t) \times \Delta t} \times 100\% \quad \forall t \in T \tag{31}$$

where $P_{gen}(t)$ is the electricity generation at time t, $T_{gen}(t)$ is the thermal energy generation at time t, and Δt is the simulation time step.

B. LOSS OF POWER SUPPLY PROBABILITY (LPSP)

When the system demand is greater than the generation, the system experiences a loss of power supply. It is necessary to keep the loss of power supply within a specific margin for ultimate system reliability. The lower value of LPSP defines a more reliable system. Hence, LPSP is also considered as a constraint in the optimization problem.

LPSP is the ratio of summation of power shortage at each time step and summation of demand at each time step. The minimum and maximum values of LPSP are 0 and 1, respectively. Equation (32-35) present the expression for both electric and thermal LPSP.

$$LPSP_e = \frac{\sum_{t=1}^{T} (P_{dem}(t) - P_{gen}(t))}{\sum_{t=1}^{T} P_{EL}(t)} \times 100\% \quad P_{dem}(t) > P_{gen}(t) \tag{32}$$

$$P_{dem}(t) = P_{EL}(t) + P^{min}_{BES,SOC}(t) + P^{min}_{Htank,SOC}(t) \quad \forall t \in T \tag{33}$$

$$LPSP_t = \frac{\sum_{t=1}^{T} (T_{dem}(t) - T_{gen}(t))}{\sum_{t=1}^{T} P_{TL}(t)} \times 100\% \quad T_{dem}(t) > T_{gen}(t) \tag{34}$$

$$T_{dem}(t) = P_{TL}(t) + P^{min}_{TES,SOC}(t) \quad \forall t \in T \tag{35}$$

where $P^{min}_{BES,SOC}(t)$, $P^{min}_{Htank,SOC}$, $P^{min}_{TES,SOC}(t)$ are the necessary power to maintain minimum SOC of the BES (kW), minimum power required for generating hydrogen to support the minimum SOC of hydrogen tank (kW), and required power to maintain minimum SOC of the TES (kW), respectively.

C. SURPLUS ENERGY FRACTION (SEF)

It is requisite to maintain surplus energy within a nuclear-renewable HES for optimal planning. Due to the intermittent characteristics of RESs, it is quite impossible to keep zero SEF. However, SEF must be limited to a particular percentage. A larger percent of SEF is not acceptable for an optimal and reliable energy system. The SEF is determined by (36-39) for both electric and thermal energy [86], [87].

$$SEF_e = \frac{\sum_{t=1}^{T} \left(P_{gen}(t) \times \Delta t - P_{con}(t) \times \Delta t\right)}{\sum_{t=1}^{T} P_{gen}(t) \times \Delta t} \times 100\% \quad P_{gen}(t) > P_{con}(t) \tag{36}$$

$$P_{con}(t) = P_{EL}(t) + P^{max}_{BES,SOC}(t) + P^{max}_{Htank,SOC}(t) \quad \forall t \in T \tag{37}$$

$$SEF_t = \frac{\sum_{t=1}^{T}\left(T_{gen}(t)\times\Delta t - T_{con}(t)\times\Delta t\right)}{\sum_{t=1}^{T} T_{gen}(t)\times\Delta t}\times 100\%$$
$$T_{gen}(t) > T_{con}(t) \quad (38)$$

$$T_{con}(t) = P_{TL}(t) + P^{max}_{TES,SOC}(t) \quad \forall t \in T \quad (39)$$

where $P^{max}_{BES,SOC}(t)$, $P^{max}_{Htank,SOC}(t)$, $P^{max}_{TES,SOC}(t)$ are the necessary power to maximize the BES's SOC, required power to maximize the hydrogen storage's SOC, and required power to maximize the TES's SOC, respectively.

D. COST OF ENERGY (COE)

COE is the expenses associated with the generation of energy per kWh. It helps to compare different technologies that have uneven installation cost, capacities, lifetime, and return. Equation (40) calculates the COE of an energy system [88].

$$COE = \frac{NPC_{total}}{\sum_{t=1}^{8760}(P_{EL}(t)+P_{TL}(t))\times\Delta t}\times\frac{i(1+i)^N}{(1+i)^N-1} \quad (40)$$

where NPC_{total} is the system total Net Present Cost (NPC) ($), i is the real interest rate (%), and N is the project lifetime (years).

E. LEVEL OF AUTONOMY (LA)

Level of Autonomy (LA) defines the percentage of duration when the loss of load does not occur within the energy system. The higher value of LA implies a more reliable system. The minimum and maximum value of LA could be 0% and 100%, respectively. Equation (41-42) represents the LA of an energy system [88].

$$LA_e = 1 - \frac{H^e_{LOL}}{H_{total}}\times 100\% \quad (41)$$

$$LA_t = 1 - \frac{H^t_{LOL}}{H_{total}}\times 100\% \quad (42)$$

where H^e_{LOL} is the total number of hours when a loss of electricity occurs (hours), H_{total} is the entire operation hour of the HES (hours), and H^t_{LOL} is the total number of hours when a loss of thermal power occurs (hours).

VI. OPTIMIZATION MODEL

A. OBJECTIVE FUNCTION

A single-objective N-R MHES planning problem is addressed in this paper to minimize the system NPC. The optimization problem formulation consolidates technical and economic parameters. LPSP, SEF, and other technical parameters are employed as constraints in the optimization problem. The objective function is the sum of all system components' NPC. The fitness function of the minimization problem is expressed by (43). Typically, the NPC of any equipment is the summation of the present value of total capital cost, replacement cost, O&M cost, and fuel cost. MMR has additional decommissioning cost and refueling cost. Thus, the decommissioning cost and the refueling cost will be zero for other components.

$$\mathbf{min}\ f_{NPC} = \sum_{i\in G} C^i_{cap} + C^i_{rep} + C^i_{O\&M} + C^i_{fuel} + C^{MMR}_{dec} + C^{MMR}_{refuel} - C^i_{salv} \quad \forall i \in G \quad (43)$$

Capital cost occurs at the beginning of the project lifespan. It is determined once in the whole project lifespan. The capital cost of any equipment (except MMR) is calculated as follows.

$$C^i_{cap} = N^i_{com}\times C^{unit(i)}_{cap} \quad \forall i \in G \quad (44)$$

The capital cost of MMR starts decreasing with lessons learned since MMR is the first-of-a-kind product. Therefore, the capital cost of MMR is calculated differently in this paper. Equation (45) determines the MMR cost as follows.

$$C^{MMR}_{cap} = \sum_{n=1}^{N_{MMR}} C^{MMR(1st)}_{cap}\times(N_{MMR})^R \quad (45)$$

The replacement cost occurs at the end of a component lifespan. The number of replacements depends on the equipment lifetime and the project lifespan. The replacement cost (present value) of a system equipment is determined by (46-49).

$$C^i_{rep} = N^i_{com}\times\sum_{n=1}^{N_{rep}} C^{unit(i)}_{rep}\times\frac{1}{(1+r)^{j_{rep}}} \quad \forall i \in G \quad (46)$$

$$N_{rep} = ceil\left(\frac{T_{PL}}{LT^i_{com}}\right) - 1 \quad (47)$$

$$r = \frac{i' - f}{1+f} \quad (48)$$

$$j_{rep} = \sum_{n=1}^{N_{rep}} 1 + \left(n\times LT^i_{com}\right) \quad (49)$$

The O&M cost of equipment is associated with operating and maintaining that equipment. In this paper, O&M's annual value is regarded to determine the entire present worth of the O&M cost for each component. Annual O&M cost is identical though the whole project lifespan. Equation (50) defines the present value of the O&M cost for a component.

$$C^i_{O\&M} = N^i_{com}\times C^{annual(i)}_{O\&M}\times\frac{\left[(1+r)^{T_{PL}}\right]-1}{r(1+r)^{T_{PL}}} \quad \forall i \in G \quad (50)$$

The fuel cost is the cost associated with fueling the generator. Though RESs do not have fuel cost, MMR has fueling cost. The present worth of MMR fuel cost is calculated by (51).

$$C^i_{fuel} = C^{annual(i)}_{fuel}\times\frac{\left[(1+r)^{T_{PL}}\right]-1}{r(1+r)^{T_{PL}}} \quad \forall i \in G \quad (51)$$

The salvage value is the remaining value of the equipment at the end of the project lifespan. Linear depreciation is assumed in this study to calculate salvage value, implying a proportional relationship with the component's remaining

lifespan. Equation (52-54) determines the salvage value of a component [89].

$$LT^{i}_{rep} = LT^{i}_{com} \times \text{floor}\left(\frac{T_{PL}}{LT^{i}_{com}}\right) \quad \forall i \in G \tag{52}$$

$$LT^{rem}_{com(i)} = LT^{i}_{com} - (T_{PL} - LT^{i}_{rep}) \tag{53}$$

$$C^{i}_{salv} = C^{unit(i)}_{rep} \times \frac{LT^{rem}_{com(i)}}{LT^{i}_{com}} \tag{54}$$

The decommissioning cost is accumulated uniformly throughout the project lifespan. Equations (55) calculates MMR decommissioning cost as follows.

$$C^{MMR}_{dec} = C^{MMR(annual)}_{dec} \times \frac{\{(1+r)^{T_{PL}}\} - 1}{r(1+r)^{T_{PL}}} \tag{55}$$

The fuel module of MMR is replaced every ten years of interim. Therefore, the MMR refueling cost occurs every ten years interval. It should be mentioned that the first year of the MMR installation also includes refueling cost since the factory-built MMR fuel module is also brought to the licensed-site in the first year. Equation (56-58) determines the MMR refueling cost.

$$C^{MMR}_{refuel} = N_{MMR} \times \sum_{n=1}^{N_{refuel}} C^{MMR(unit)}_{refuel} \times \frac{1}{(1+r)^{j_r}} \tag{56}$$

$$N_{refuel} = \text{ceil}\left(\frac{T_{PL}}{LT^{MMR}_{fuel}}\right) \tag{57}$$

$$j_r = \sum_{n=1}^{N_{refuel}} 1 + \left(n \times LT^{MMR}_{fuel}\right) \tag{58}$$

B. CONSTRAINTS

The optimization problem incorporates several constraints to ensure the utmost reliability of the HESs. Power generation by any source must be less or equal to the maximum capacity of the source. It can be presented as follows.

$$P^{i}_{gen}(t) \le P^{i}_{gen,max} \quad \forall i, \forall t \tag{59}$$

$$T^{i}_{gen}(t) \le T^{i}_{gen,max} \quad \forall i, \forall t \tag{60}$$

The total system's production must be equal or greater to the total system requirements. The energy balance constraints are presented in (61-64).

$$\sum P^{y}_{gen}(t) \ge \sum_{t=1}^{T} P^{y}_{EL}(t) \quad \forall t \in T, \forall y \tag{61}$$

$$\sum T^{y}_{gen}(t) \ge \sum_{t=1}^{T} P^{y}_{TL}(t) \quad \forall t \in T, \forall y \tag{62}$$

$$\sum P^{y}_{gen}(t) = \sum_{t=1}^{T} N_{PV} P_{PV}(t) + \sum_{t=1}^{T} N_{WT} P_{W}(t) + \sum_{t=1}^{T} N_{MMR} P_{MMR}(t) + \sum_{t=1}^{T} P_{HT}(t) + \sum_{t=1}^{T} P_{BG}(t) \quad \forall t \in T, \forall y \tag{63}$$

$$\sum T^{y}_{gen}(t) = \sum_{t=1}^{T} N_{MMR} T_{MMR}(t) + \sum_{t=1}^{T} T_{BG}(t) \quad \forall t \in T, \forall y \tag{64}$$

Equation (65-67) are employed to hydrogen storage, BES, and TES, respectively, as constraints to ensure the resilient performance of the storage systems.

$$Htank^{min}_{SOC} \le Htank^{y}_{SOC}(t) \le Htank^{max}_{SOC} \quad \forall t \in T, \forall y \tag{65}$$

$$BES^{min}_{SOC} \le BES^{y}_{SOC}(t) \le BES^{max}_{SOC} \quad \forall t \in T, \forall y \tag{66}$$

$$TES^{min}_{SOC} \le TES^{y}_{SOC}(t) \le TES^{max}_{SOC} \quad \forall t \in T, \forall y \tag{67}$$

LPSP and SEF are the two most essential reliability parameters incorporated into the optimization problem as constraints. The reliability parameter values must remain within the specified limits, as presented in (68-71).

$$LPSP_e \le LPSP^{max}_{e} \tag{68}$$

$$LPSP_t \le LPSP^{max}_{t} \tag{69}$$

$$SEF_e \le SEF^{max}_{e} \tag{70}$$

$$SEF_t \le SEF^{max}_{t} \tag{71}$$

The maximum LPSP and SEF value is set to 5% and 10%, respectively, in the optimization problem. These are the typically acceptable limits of LPSP and SEF for a reliable HES [86], [73].

C. DECISION VARIABLES

The optimization problem intends to find out the optimal configuration of the three distinct N-R MHESs. The identified decision variables are no. of PV panel, no. of WT, no. of MMR, size of the hydro plant (kW), no. of hydrogen tank, size of BES and TES (kWh), size of E2H and H2E unit (kW), and the required CHP unit efficiency (%). The decision variables of the problem can be written as follows.

$$0 \le N_{PV} \le N^{max}_{PV} \quad N_{PV} \in \mathbb{Z} \tag{72}$$

$$0 \le N_{WT} \le N^{max}_{WT} \quad N_{WT} \in \mathbb{Z} \tag{73}$$

$$0 \le N_{MMR} \le N^{max}_{MMR} \quad N_{MMR} \in \mathbb{Z} \tag{74}$$

$$0 \le N_{Htank} \le N^{max}_{Htank} \quad N_{Htank} \in \mathbb{Z} \tag{75}$$

$$0 \le HT_{cap} \le HT^{max}_{cap} \tag{76}$$

$$0 \le BES_{cap} \le BES^{max}_{cap} \tag{77}$$

$$0 \le TES_{cap} \le TES^{max}_{cap} \tag{78}$$

$$0 \le \eta^{MMR}_{CHP} \le \eta^{MMR(max)}_{CHP} \tag{79}$$

D. IMPLEMENTATION OF OPTIMIZATION ALGORITHM

The PSO algorithm's formulation is inspired by the nature of the social organism, e.g., fish, birds, and ant colonies. PSO emulates information-sharing behavior. PSO finds the optimal solution by using swarm particles. The particles move randomly and obtain their "best" and group "best" position.

Then, the particles compare their best values and find the optimal solution.

The particle alters its position based on the new velocity. The position and velocity are changed according to (80-82) [90].

$$v_i^{t+1} = \omega\left[v_i^t + c_1 r_1\left(xBest_i^t - x_i^t\right) + c_2 r_2\left(gBest_i^t - x_i^t\right)\right] \quad (80)$$

$$x_i^{t+1} = x_i^t + v_i^t.t \quad (81)$$

$$\omega = \frac{2}{\left|2 - \varphi - \sqrt{\varphi^2 - 4\varphi}\right|}, \quad \varphi = c_1 + c_2 > 4 \quad (82)$$

where i, x_i, and v_i denote particle, position vector of the particle, and velocity vector of the particle, respectively. xBest and gBest are the particle best position and group best position, sequentially. ω, c_1, and c_2 are constriction coefficient, individual acceleration coefficient (2.05), and social acceleration coefficient (2.05), respectively. r_1 and r_2 are the random number within [0, 1].

Fig. 11 outlines the implementation process of the PSO algorithm. In the beginning, the PSO algorithm reads the input data, e.g., system load profile, resources data, and economic parameters of the component. Then, it initializes the iteration number, population size, and the number of individual runs. PSO algorithm also sets the acceleration coefficient, inertia coefficient, constriction coefficient, constraints, and limits of the variables. The upper bound of the MMR, PV panels, WT, hydro plant capacity (kW), CHP efficiency of MMR (%), hydrogen tank, BES (MWh), and TES (MWh) are 10, 100, 100, 1000.64, 30, 25, 100, and 25, respectively. The algorithm then evaluates each particle until it finds the global best values, as illustrated in Fig. 11. Equation (80-82) are used to update the positions and velocities of the particles. A static penalty function is also employed with the objective function. Once the constraints are violated, a fixed value will be added to the objective function no matter how much the violations are.

VII. SIMULATION AND RESULTS

An adequate number of population (250) and iterations (300) are considered in the PSO optimization. The results of PSO assert that the "Multiple Resources and Multiple Products-based coupled N-R MHES (Case-03)" provides the lowest NPC ($ 79.33 million), whereas the NPC of "Directly coupled N-R MHES (Case-01)" is the highest ($ 141.31 million). The "Single Resource and Multiple Products-based coupled N-R MHES" is denoted as "Case-02" in this paper. The NPC of the three cases is shown in Fig. 12.

Table 2 records the details of the optimal configuration of three N-R MHESs. Case-03 includes the least number of MMR since renewable generation is available in this case. On the other hand, Case-01 combines the highest number of MMRs since the CHP unit is not available, and the total system demand is supported by only electricity. A maximum number (100) of solar PV panels are utilized in Case-01 and Case-03 since the availability of solar irradiance at the project location is reasonable. Case-02 and Case-03 disregard the BES in the system architecture as hydrogen storage is sufficient to manage the system demand. The PSO algorithm does not suggest including any E2H and H2E units in any of the system configurations.

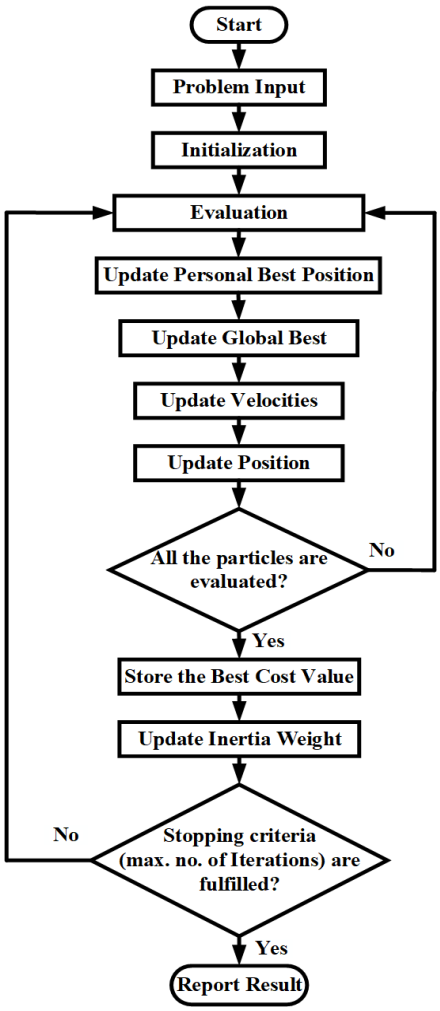

FIGURE 11. Implementation of the PSO algorithm.

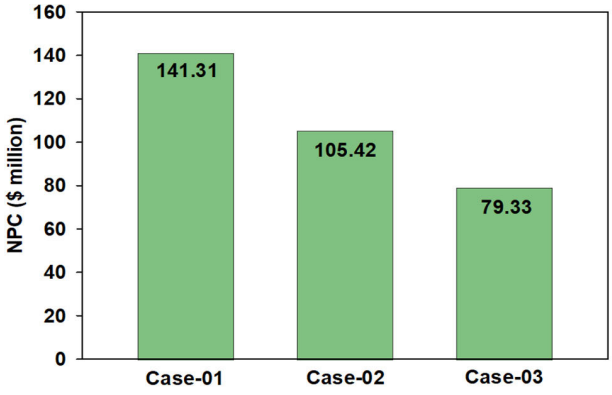

FIGURE 12. Comparison of NPC for the proposed N-R MHESs.

TABLE 2. Optimal configuration of different proposed N-R MHES.

Cases	Case-01	Case-02	Case-03
Number of particles	250	250	250
Number of iterations	300	300	300
Number of MMR	6	5	3
Number of PV panels	100	N/A[1]	100
Number of WT	77	N/A	34
Hydro turbine capacity (kW)	390.25	N/A	1000.64
Required efficiency of CHP unit (%)	N/A	16.8	24.6
Number of hydrogen tank	25	22	23
BES capacity (MWh)	4.97	0	0
TES capacity (MWh)	N/A	19.90	19.90
BG capacity (kW)	65.10	65.10	65.10
E2H unit capacity (kW)	0	0	0
H2E unit capacity (kW)	N/A	0	0

[1]Not applicable

Although Case-02 comprises five MMR units in the system, the PSO optimization suggests running one unit at 32% of its rated power; this is one vital drawback of the stand-alone MMR-based energy system (Case-02). If all the five units operate at maximum capacity, the SEF will be larger than the defined boundary, and the reliability constraint will be violated. This situation may also include large-scale energy storage systems to store the excess generation with an additional storage cost. Load-following MMR may overcome the sizing of energy storage systems in this case, but the NPC will still be high due to MMR's substantial capital cost. On the other hand, if four MMR units have been incorporated within the system, the LPSP will be higher than the specified limit. Thus, the reliability constraint will also be violated. Since it is required to determine an integer number of MMR units, the PSO selects five MMR units; one of them will run less than its rated capacity. As a significant fraction of MMR total deployment cost is related to sunk cost, the NPC will be roughly comparable whether one of the MMR units runs at 32% of its rated capacity or operates at its full capacity. Therefore, the operation of Case-02 is not a profitable investment, and it is challenging for variable energy demand. It should be noted that MMR units run at the nominal capacity for Case-01 and Case-03.

Table 3 presents the KPIs considered in the paper. No separate LPSPs, e.g., $LPSP_{elec}$ and $LPSP_{ther}$, are calculated for Case-01 since the electric and the thermal demand are fulfilled simultaneously by utilizing only electric power. Case-01 considers the electrical demand and the thermal demand as a single entity. The maximum allowable limits of LPSP and SEF are 5% and 10% in the optimization problem. Literature reviews found the specified limits of LPSP and SEF. If HES has the LPSP and SEF within the defined limits, the system is considered as reliable and resilient. All the system arrangements, recorded in Table 3, have the values of LPSP and SEF within the defined limits, signifying the reliability for all cases. However, electric LPSP and SEF of Case-03 are the lowest (4.36% and 1.83%, respectively), referring to the most reliable system. If the GRF is higher

TABLE 3. KPIs of different proposed N-R MHES.

Parameters	Case-01	Case-02	Case-03
$LPSP_{elec}$ (%)	5	5	4.36
$LPSP_{ther}$ (%)		5	5
SEF_{elec} (%)	10	3.45	1.83
SEF_{ther} (%)		10	10
GRF_{elec} (%)	125.97	118.48	116.48
GRF_{ther} (%)		108.71	108.71
LA_{elec} (%)	85.42	89.93	90.97
LA_{ther} (%)		83.68	79.51
COE ($/kWh)	0.2072	0.1545	0.1163

than 100% and as much as close to 100%, the system is considered as reliable in terms of GRF. Therefore, Case-03 is also identified as the most reliable system in terms of GRF (GRF_{elec} and GRF_{ther} are 116.48% and 108.71%, respectively). However, Case-02 shows the same thermal GRF as Case-03. The higher value of LA offers better resiliency and operability of the system. Hence, Case-03 (90.97) and Case-02 (83.68) indicates the highest resiliency in terms of LA_{elec} and LA_{ther}, respectively.

Fig. 13 presents the PSO convergence plot of Case-01 for the best solution. The swarms reach the optimal value with the progression of the iteration number. The best solution is obtained by 100 independent runs of the PSO program. PSO is a natural-inspired optimization algorithm, and the problem contains several constraints. Thus, PSO shows slightly different values in each run. Therefore, it is imperative to run the PSO program multiple times and identify the best results from the various runs. One hundred individual run is a reasonable approximation to get a satisfactory solution.

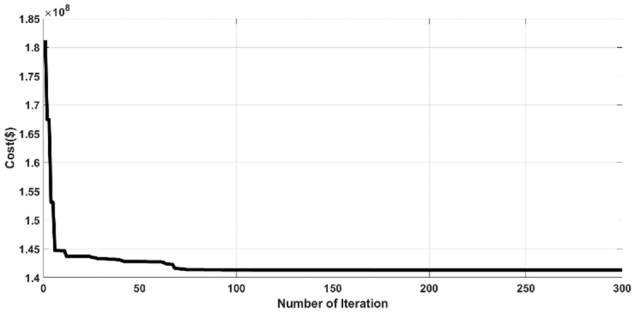

FIGURE 13. Convergence plot (Case-01).

Fig. 14 represents the total energy generation and consumption scenario of Case-01. The figure shows that energy production, along with the support of the energy storage systems, is following the demand. However, there will be a small deficit or excess power within the system due to the allowable LPSP and SEF limits. Fig. 15 depicts the charging and discharging mechanism of the energy storage systems based on the defined energy management algorithm in the earlier section. The TES is absent in Case-01 since thermal energy production is not possible in this case.

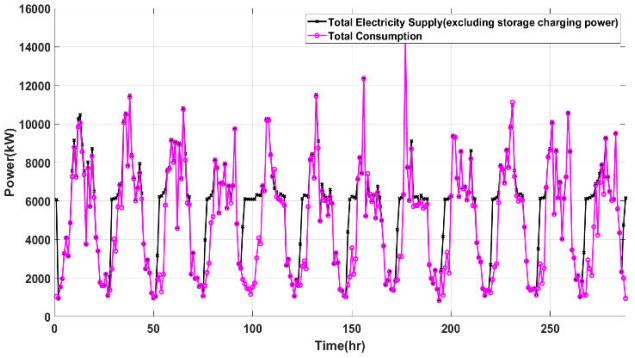

FIGURE 14. Total energy generation and consumption scenario (Case-01).

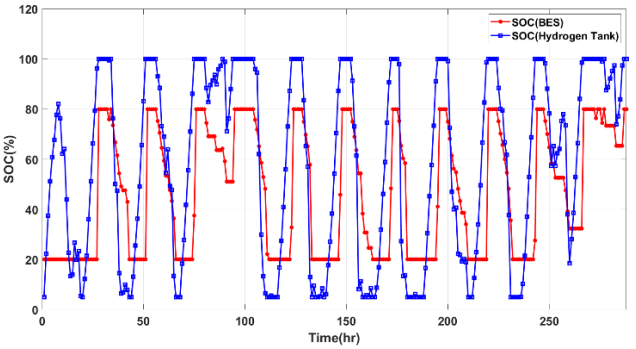

FIGURE 15. Energy storage operation (Case-01).

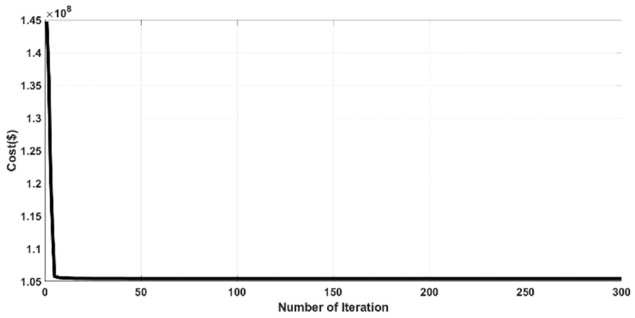

FIGURE 16. Convergence plot (Case-02).

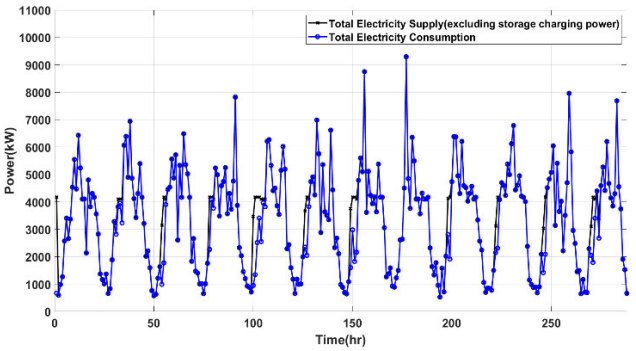

FIGURE 17. Total electric energy generation and consumption scenario (Case-02).

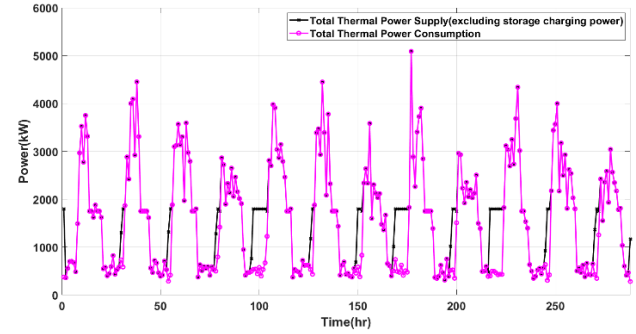

FIGURE 18. Total thermal energy generation and consumption scenario (Case-02).

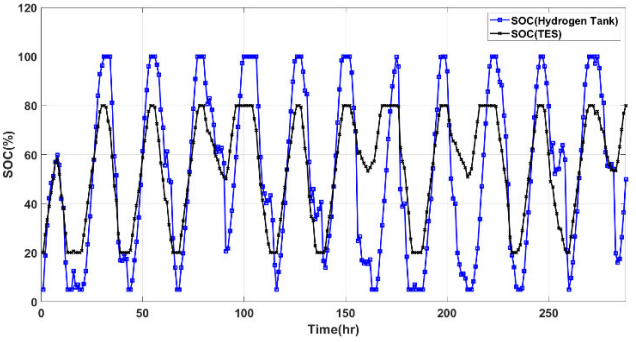

FIGURE 19. Energy storage operation (Case-02).

Fig. 16 shows the PSO convergence plot of the best run for Case-02. The particles move towards the optimal value very quickly. The multiple independent runs produce almost the same fitness value at each run. Fig. 17 represents the total electric power generation and consumption scenario of Case-02. The electrolyzer, hydrogen tank, and FC contribute to follow the variable electrical demand based on the energy management algorithm. Fig. 18 illustrates the thermal power generation and consumption scenario. TES always supports to meet the thermal demand by absorbing the excess thermal energy and delivering the required thermal power. The electric and the thermal demand have surplus and deficit power due to the permissible limits of LPSP and SEF constraints. Fig. 19 illustrates the charging and discharging scheme of the hydrogen tank and TES.

Fig. 20 illustrates the PSO convergence plot for Case-03. The particles are able to find the optimal NPC efficiently with less number of iterations. Similar to Case-02, Fig. 21 and Fig. 22 represent the electric and thermal power generation and consumption processes, respectively. Both the figures show that the production, along with the energy storage systems, is almost always achieving the system demand. Fig. 23 shows the charging and discharging scheme of hydrogen tanks and TES. The energy storage systems always accompany the demand by maintaining the minimum and maximum SOC of the storage.

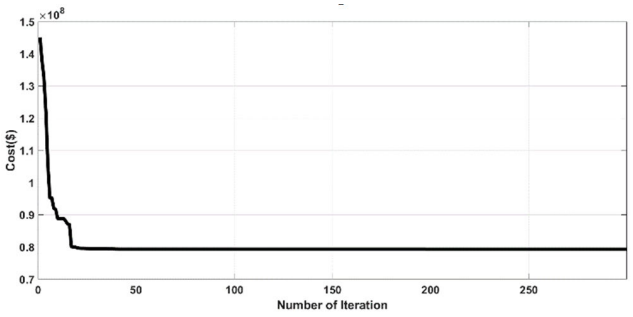

FIGURE 20. Convergence plot (Case-03).

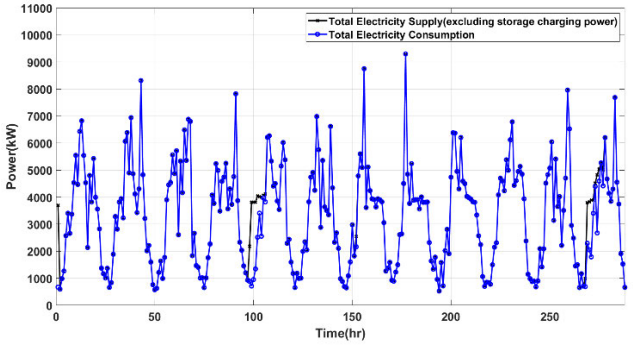

FIGURE 21. Total electric energy generation and consumption scenario (Case-03).

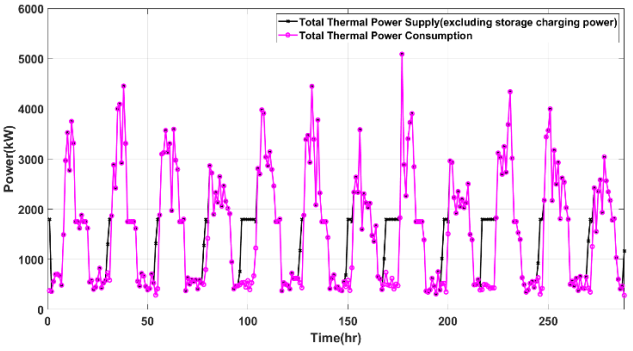

FIGURE 22. Total thermal energy generation and consumption scenario (Case-03).

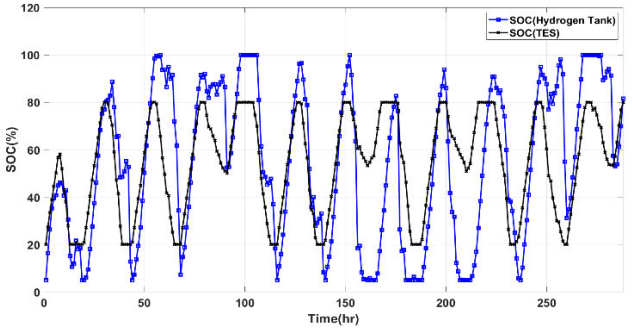

FIGURE 23. Energy storage operation (Case-03).

Since a nuclear-renewable integrated system's performance depends on several variables, the later subsections discuss the sensitivity of system performance to different parameters. The sensitivity analysis validates the outcomes obtained from the base case analysis. The sensitivity analysis also investigates the impact of various parameters on system economic, reliability, and resiliency. A sensitivity assessment is crucial for a system modeler to model, analyze, and develop the system infrastructure. The most influential parameters are identified in the sensitivity analysis. It helps the research community for future research and development. Several system variables are selected for the sensitivity assessment and presented in later subsections. Table 4 summarizes the main concepts of the sensitivity analysis conducted in this section.

TABLE 4. A summary of the sensitivity analysis.

Subsection	Summary
A	This part evaluates the sensitivity of the variation in daily peak demand to NPC.
B	The subsection assesses the sensitivity of the variation in annual peak demand to NPC.
C	This portion of the analysis explores the impact of average demand changes on system NPC.
D	The subsection assesses and identifies the influence of different equipment cost on NPC.
E	This subsection determines the impact of system economic parameters, such as nominal discount rate, inflation rate, and project lifetime, on NPC.
F	This part evaluates the impact of MMR capacity factor on system configuration and system NPC.

A. ASSESSMENT OF SENSITIVITY TO SHIFTING OF DAILY PEAK DEMAND

Though the peak occurs (both electric and thermal demand) at mid-day in the base cases, it is also reasonable that the peak may occur at the beginning or end of the day. The peak demand for any load depends on the types of load and the project location. Usually, wind speed does not reach zero-level at night, while there will be no solar irradiance at night. Hence, alterations in peak demand cause inclusion or reduction of generation sources depending on the geographical region and the level of system demand. Therefore, a sensitivity analysis has been conducted in this subsection by shifting the peak demand (both electric and thermal demand) by 12 hours. Fig. 24 and Fig. 25 present the shifted peak scenarios of the electrical and the thermal demand, respectively.

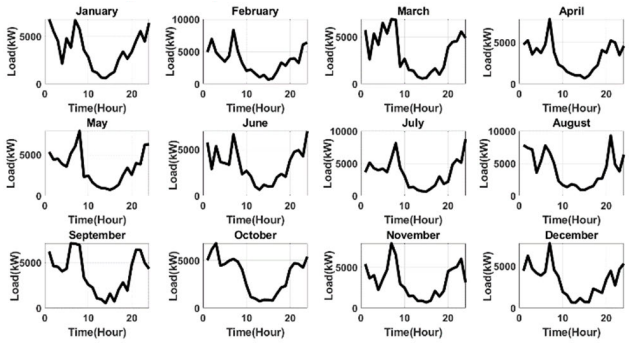

FIGURE 24. Shifted electric peak demand (daily).

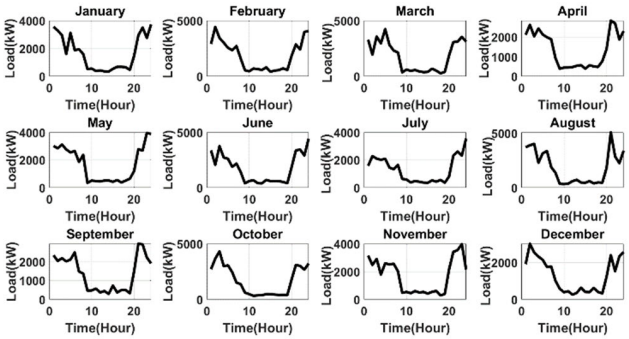

FIGURE 25. Shifted thermal peak demand (daily).

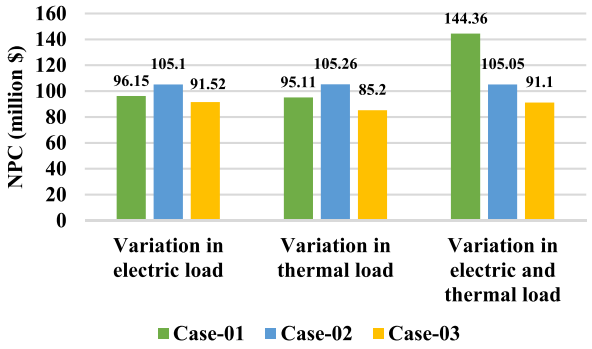

FIGURE 26. Impact of variation in daily peak demand.

Fig. 26 represents the differences in NPC of three nuclear-renewable hybridized systems due to variation in system peak. The system peak variation analysis is divided into three parts: variation in electric load, variation in thermal load, and variation in both electrical and thermal load. From all the cases of system peak variation, Case-03 provides the lowest system NPC. Case-02 shows higher NPC than Case-01 in the first and second parts. Since Case-01 and Case-03 include renewables and the demand profile is changing, indeed, the NPC will change due to the inclusion or reduction of different renewable generation sources. Therefore, the NPC of Case-01 and Case-03 are varied in Fig. 26 compared to the base case NPC mention in Fig. 12. The variation of daily peak demand insignificantly affects the NPC of Case-02 because of the continuous and scheduled mode of generation by MMR and BG, respectively. The PSO always recommends to include five MMR units for Case-02 in all types of variation, while one of the units will run at between 27-32% of its rated capacity. Hence, the NPC of Case-02 does not change due to the peak variation in electric demand, or thermal demand, or both. The NPC of Case-02 for daily peak variation (electric, thermal, or both) is almost similar to base case NPC. The TES cost is accountable for the slight changes in NPC for Case-02 since the sizing of the TES changes with the variation in demand. The reliability parameters are regarded as optimization constraints, and the system resiliency is maintained in all cases.

B. ASSESSMENT OF SENSITIVITY TO SHIFTING OF SEASONAL DEMAND

In the base case analysis, the electric and thermal peak occurs nearby the month of July-August. The seasonal peak demand also depends on the type of load and applications. Hence, the seasonal peak demand is shifted by six months in this subsection, implying that the annual peak will occur at the staring of the year (around January) in the shifted load demand. Fig. 27 and Fig. 28 present the electric and thermal seasonal shifted load profiles, respectively.

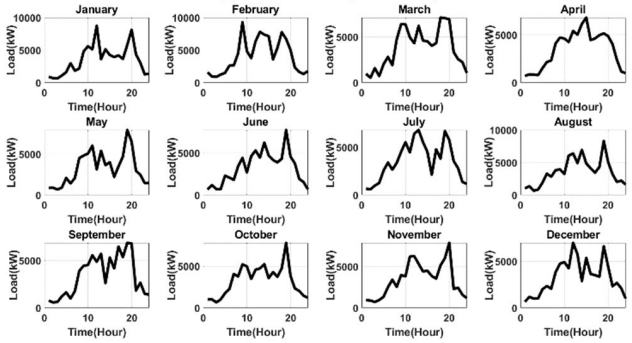

FIGURE 27. Shifted electric peak demand (seasonal).

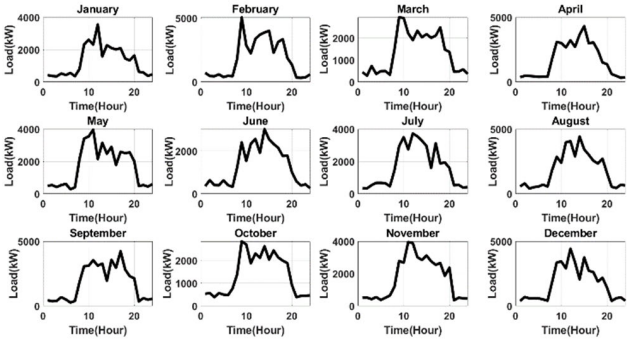

FIGURE 28. Shifted thermal peak demand (seasonal).

Similar to the previous subsection, this subsection also divided the sensitivity analysis into three parts. The simulation results also reveal the lowest NPC for Case-03 and the highest NPC for the Case-01 in all sections. Fig. 29 summarizes the sensitivity assessment results due to the annual peak demand variation. The seasonal peak variation does not affect the NPC of Case-02 and Case-03. Therefore, the NPC for Case-02 and Case-03 presented in Fig. 29 is almost similar to the base case. The seasonal peak variation affects the Case-01 since the electric and thermal load is viewed as a single demand in Case-01; any difference either in electrical demand or thermal demand alter the NPC.

As Case-02 consists of nuclear and BG, the system peak (daily and yearly) variations cannot affect the optimal system configuration and the NPC significantly. PSO includes five MMR units in all types of peak variation in Fig. 29. PSO also recommends running one of the MMR units to run at 30% of

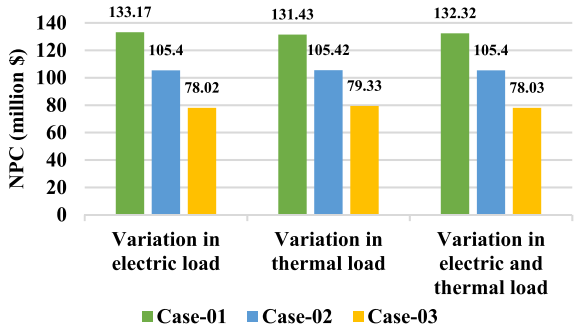

FIGURE 29. Impact of variation in seasonal peak demand.

its maximum capacity for Case-02. The sizing of TES always remains the same in this sensitivity analysis for Case-02. Thus, the NPC for Case-02 is the same for seasonal electric demand peak variation, or seasonal thermal peak variation, or both. On the other hand, since Case-01 and Case-03 includes a considerable number of renewables, seasonal peak variation affects the optimal system architecture and the NPC, as shown in Fig. 29.

It should be mentioned that there is a positive co-relationship between typical system demand and availability of the renewables, e.g., solar irradiance and wind speed. It indicates that all the solar irradiance, wind speed, and peak demand usually reach the maximum at the same time, mid-day, in a day. Therefore, daily peak variation impacted more severely than seasonal peak variation, as presented in Fig. 26 and Fig. 29.

C. ASSESSMENT OF SENSITIVITY TO VARIATION IN AVERAGE ENERGY DEMAND

The average electric and thermal demand may rise or decrease by a certain percentage at any time or throughout a particular duration. Therefore, a sensitivity analysis is carried out in this subsection by increasing and decreasing the electric and thermal demand by 10%.

Fig. 30, Fig. 31, and Fig. 32 represent the diversity of NPC due to changes in the average electric demand, the thermal demand, and both electrical and thermal demand, respectively, by ±10%. The results show that Case-03 provides the most economical NPC despite increasing or decreasing the electric and thermal demand by a certain amount. The results also imply that the directly coupled system (Case-01) has the highest NPC for all cases. Fig. 30 tells that the NPC of all cases increases proportionately with the increase in electric demand. The augmentation of electrical demand adds more generation components or storage, which ultimately increase the NPC. However, the extension of electric demand does not always affect the NPC of Case-02 evenly. The scenario, where the electrical demand is decreased by 10%, comprises four MMR units running at full capacity. Conversely, the base case and the 10% increase in electric demand include five MMR units. For the base case, one of the MMR units runs at 32% of its nominal capacity. For the 10% increase of electric demand, one of the MMR operates at 72% of its rated power, and PSO includes more hydrogen storage in this case. Hence, the NPC ($ 107.53 million) increases due to the inclusion of additional hydrogen storage systems. The sizing of the TES remains the same as the base case.

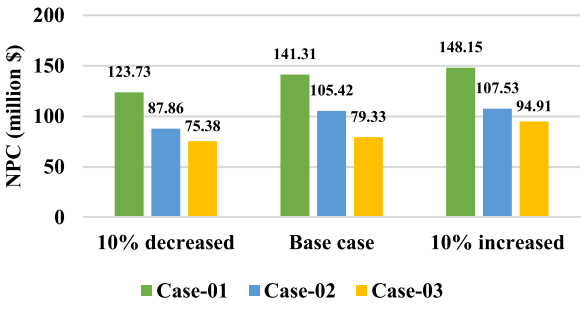

FIGURE 30. Impact of variation in average electric demand.

Thermal demand variation, illustrated in Fig. 31, does not affect Case-02 and Case-03 significantly due to the CHP unit of MMR. The CHP unit has no additional cost; the CHP unit cost is already incorporated within the component. The optimization only identifies the required efficiency of the CHP unit to fulfill the thermal demand. The PSO selects the same number of MMR units for any kind changes in thermal demand in this case; hence, the NPC of Case-02 is equal in all stages in Fig. 31. However, TES contributes to fluctuations in NPC due to the variation in thermal demand. Since Case-01 meets the thermal requirement by electricity, the thermal demand variation combines more electricity generation sources within N-R MHES that increase the NPC. Fig. 32 simulates both electric and thermal demand variation simultaneously. Since electrical demand is altering, the NPC increases with the increase of both demands for all three cases. However, Case-03 provides the best performance in terms of NPC for any load variation.

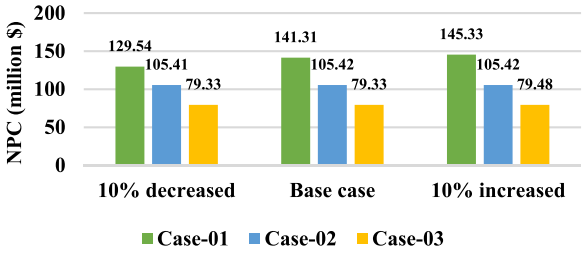

FIGURE 31. Impact of variation in average thermal demand.

D. ASSESSMENT OF SENSITIVITY TO VARIATION IN SYSTEM EQUIPMENT COST

This subsection investigates the impact of different equipment's cost on system NPC. The discussion also intends to validate the comparison results made for the base case of three proposed hybridization methods. Though HES consists of various equipment, the main components are considered

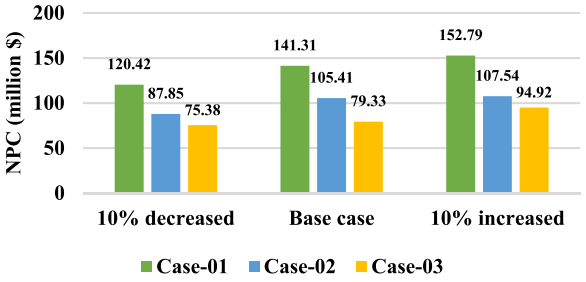

FIGURE 32. Impact of variation in both average electric and thermal demand.

in this sensitivity analysis. The overall deployment cost of a single element, such as PV panel, WT, MMR, hydro plant, BG, BES, FC, electrolyzer, and TES, is varied by ±20% of their base values. The impact of changing the component overall installation cost for Case-01 is illustrated in Fig. 33. The figure says that MMR has the highest effect on the NPC. The FC, electrolyzer, and BES also have a moderate impact on the changes in NPC. The rest of the components do not affect the system NPC significantly. The upper portion of Fig. 33 is the amplified version of the dotted part in that figure.

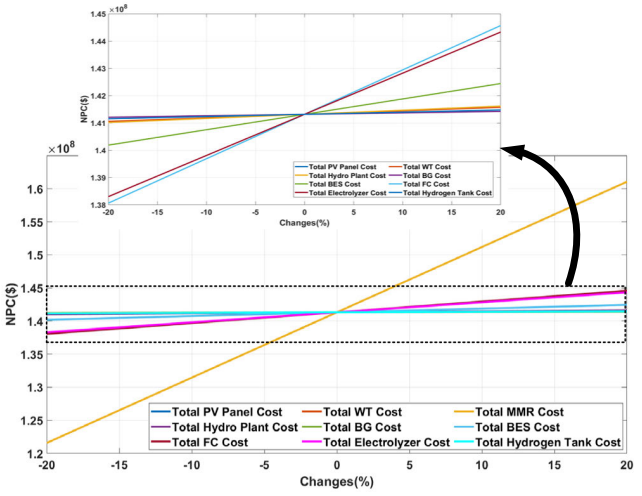

FIGURE 33. Impact of variation in system equipment cost (Case-01).

Fig. 34 depicts the effect of the various component due to the variation of the overall single component cost for Case-02. Similar to the results of Case-01, MMR has a tremendous impact on system NPC. The FC and the electrolyzer have a limited effect on the system economy, but the rest of the components have an insignificant impact on NPC.

Fig. 35 addresses that MMR has the most critical influence on the NPC, whereas the FC, electrolyzer, and hydro plant also significantly impact the system economy for Case-03. The PV panels and the TES also affect the NPC. However, the rest of the equipment has a trivial effect on NPC. By observing all the findings from the above discussion,

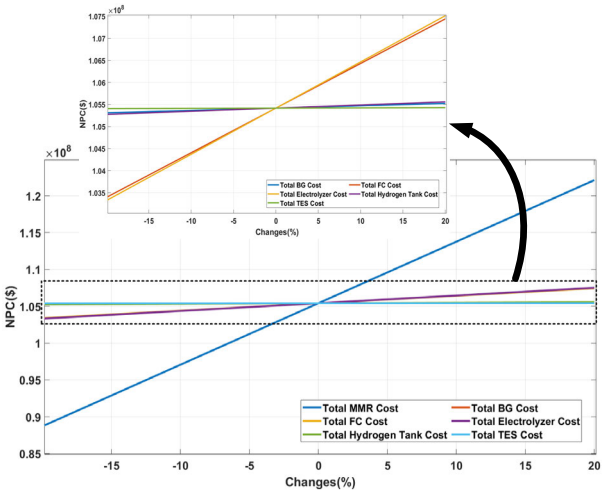

FIGURE 34. Impact of variation in system equipment cost (Case-02).

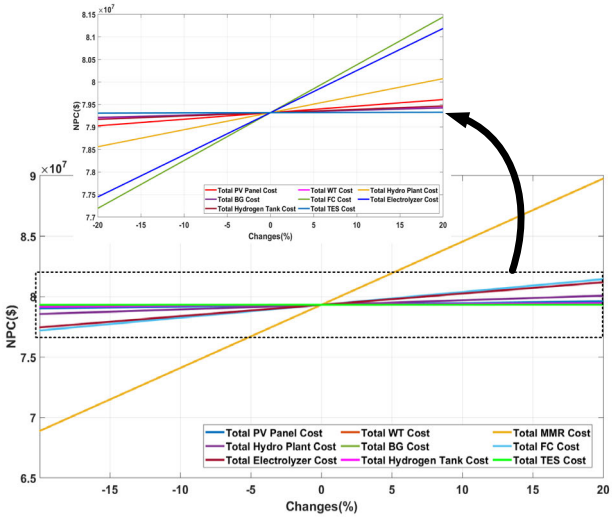

FIGURE 35. Impact of variation in system equipment cost (Case-03).

it is said that Case-03 is always superior to the other two hybridization methods for any fluctuations in equipment cost.

E. ASSESSMENT OF SENSITIVITY TO VARIATION IN ECONOMIC PARAMETERS

Project lifetime, nominal discount rate, and inflation rate are the three most important economic parameters in the techno-economic analysis of HES. The project lifetime, discount rate, and inflation rate for the base case are 40 years, 8%, and 2%, respectively.

In this section, a sensitivity analysis is conducted by differing project lifetimes, discount rates, and inflation rates from its base case. Fig. 36 summarizes the results of sensitivity to the project lifetime. The project lifetime is varied from 20 years to 100 years. The system NPC raises with the increment of the project lifetime. The NPC reaches a stable position for higher project lifetime in N-R MHES. The figure also tells that the investment in any N-R MHES is

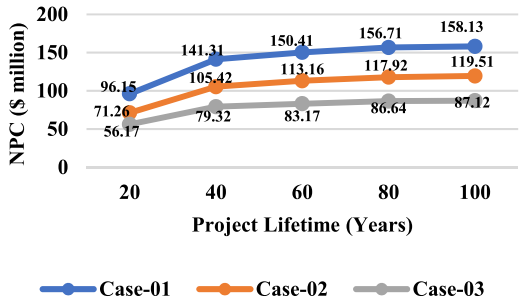

FIGURE 36. Impact of variation in project lifetime.

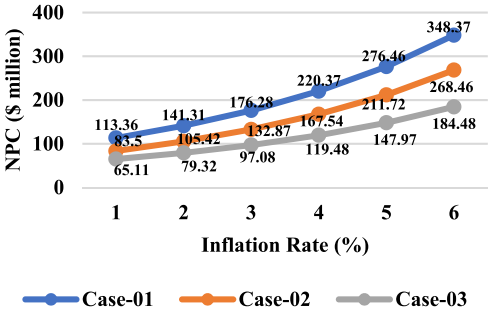

FIGURE 38. Impact of variation in inflation rate.

also financially profitable for a longer project lifetime. The results show that Case-03 has the least NPC irrespective of the project lifespan. The system reliability is also ensured by executing the reliability constraints into the optimization problem.

The discount rate is varied from 5% to 10% to evaluate the impact of the discount rate on system planning. The NPC falls with the increase in the discount rate, as shown in Fig. 37. System planners should always choose a higher discount rate for economic system modeling. The result tells that Case-03 provides the least NPC irrespective of any value of the system discount rate. The rate of changes in NPC is also more limited for the higher value of the discount rate.

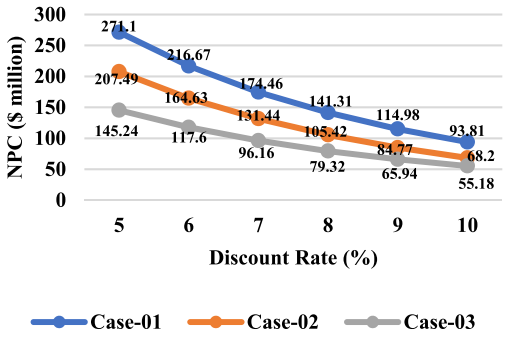

FIGURE 37. Impact of variation in discount rate.

The inflation rate is adjusted from 1% to 6% from its' base case value in this sensitivity assessment. The NPC increases significantly with the rise of the inflation rate, presented in Fig. 38. Similar to the sensitivity analysis of the project lifetime and discount rate, the NPC is lowest for the Case-03, whereas the Case-01 has the highest NPC, regardless of any value of the inflation rate. Therefore, the sensitivity assessment of the economic parameters also proves Case-03 as the most economic hybridization method for N-R MHES.

F. ASSESSMENT OF SENSITIVITY TO VARIATION IN CAPACITY FACTOR (MMR)

The capacity factor indicates how the rated capacity of a generation source is utilized in the energy system. The MMR considered in the paper may not always run at maximum rated power. Therefore, the base capacity factor (95%) would not be achieved. In this circumstance, it is inevitable to conduct a sensitivity analysis by varying the capacity factor to evaluate N-R MHESs. The goal of this evaluation is to assess the system competency for higher and lower capacity factors. The capacity factors of 65%, 75%, 85%, and 95% have been used in the sensitivity assessment.

Fig. 39 represents the NPC of the proposed N-R MHESs due to the difference in capacity factor. The NPC of all systems decreases with the increase of the capacity factor, except at 95% and 85% capacity factor for Case-02. The PSO optimization suggests seven and six MMR units for Case-02 at 65% and 75% capacity factor, respectively. On the other hand, the same number (5 units) of MMR is combined at 85% and 95% capacity factor for Case-02. Therefore, the Case-02 shows the same NPC ($ 105.42 million) at 85% and 95% of the capacity factor. However, the NPC of Case-02 at the capacity factor of 75% and 65% have been varied (120.55 million and $ 134.41 million, respectively) due to the inclusion of the different number of MMR units. Hence, the capacity factor sporadically affects the NPC depending on the demand for stand-alone MMR-based HES (Case-02). Stand-alone MMR-based HES makes the reactor selection relatively inflexible.

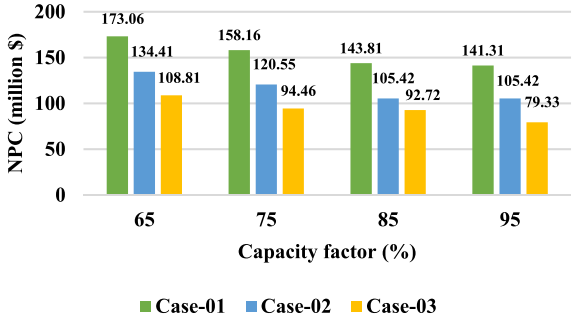

FIGURE 39. Impact of variation in capacity factor (MMR).

For Case-01 and Case-03, the reduced capacity factors allow to include more renewable generation sources. The inclusion of a few PV panels, WT, or hydro turbine can

manage the small variation of MMR Capacity. Since MMR deployment cost is very high, the optimization recommends using renewable sources rather than incorporating a new MMR unit. Therefore, the NPC of Case-01 and Case-03 are also increased with the decreasing of MMR's capacity factor. However, Case-03 provides the lowest NPC in all values of capacity factor, whereas Case-01 has the highest NPC in all cases.

VIII. CONCLUSION AND FUTURE WORK

This paper introduces three distinct nuclear-renewable hybridization approaches, i.e., "Direct Coupling," "Single Resource and Multiple Products-based Coupling," and "Multiple Resources and Multiple Products-based Coupling." The study recognizes "Multiple Resources and Multiple Products-based Coupling" as the most useful hybridization technique. The simulation results show that "Multiple Resources and Multiple Products-based N-R MHES" provides the lowest NPC ($ 79.33 million) compared to "Directly coupled N-R MHES" ($ 141.31 million) and "Single Resource and Multiple Products-based N-R MHES" ($ 105.42 million) for the base case. The results also confirm that all the systems provide an adequate margin of reliability for all the cases. The sensitivity analysis proves that "Multiple Resources and Multiple Products-based N-R MHES" remains the most effective hybridization technique despite the variation in key input parameters. "Directly coupled N-R MHES" has technical advantages, such as full resource usage, but it is not a profitable investment. "Single Resource and Multiple Products-based Coupled system" is challenging to meet the variable demand; the MMR unit's capacity is not utilized properly in this case. "Multiple Resources and Multiple Products-based Coupled N-R MHES" provides outstanding performance for dynamic load by using the resource capacity suitably. Therefore, "Multiple Resources and Multiple Products-based N-R MHES" could be the most efficient nuclear-renewable hybridization technique for demonstration and practical implementation.

Future research may include quantifying a comparison between fossil-fired MEG and N-R MHES by utilizing the most-effective hybridization technique. Since the assessment on the quality of heat generated from MMR and BG is out of scope for this paper, it should be examined and quantified in future investigations to identify specific applications. A Comprehensive licensing procedure for N-R MHES should be focused on future research as well.

REFERENCES

[1] H. Ritchie and M. Roser. (Apr. 2017). *Air Pollution*. Our World Data. Accessed: Aug. 11, 2020. [Online]. Available: https://ourworldindata.org/air-pollution

[2] H. Ritchie and M. Roser. (Mar. 2014). *Energy*. Our World Data. Accessed: Jul. 15, 2020. [Online]. Available: https://ourworldindata.org/energy

[3] H. Blanco and A. Faaij, "A review at the role of storage in energy systems with a focus on power to gas and long-term storage," *Renew. Sustain. Energy Rev.*, vol. 81, pp. 1049–1086, Jan. 2018, doi: 10.1016/j.rser.2017.07.062.

[4] J. P. Deane, B. P. Ó Gallachóir, and E. J. McKeogh, "Techno-economic review of existing and new pumped hydro energy storage plant," *Renew. Sustain. Energy Rev.*, vol. 14, no. 4, pp. 1293–1302, May 2010, doi: 10.1016/j.rser.2009.11.015.

[5] *Comparing Fuel Cell Technologies*. GenCell-Fuel Cell Generators. Accessed: Jul. 3, 2020. [Online]. Available: https://www.gencellenergy.com/news/comparing-fuel-cell-technologies/

[6] S. Suman, "Hybrid nuclear-renewable energy systems: A review," *J. Cleaner Prod.*, vol. 181, pp. 166–177, Apr. 2018, doi: 10.1016/j.jclepro.2018.01.262.

[7] H. A. Gabbar, M. R. Abdussami, and M. I. Adham, "Techno-economic evaluation of interconnected nuclear-renewable micro hybrid energy systems with combined heat and power," *Energies*, vol. 13, no. 7, p. 1642, Apr. 2020, doi: 10.3390/en13071642.

[8] J. Augutis, L. Martišauskas, and R. Krikštolaitis, "Energy mix optimization from an energy security perspective," *Energy Convers. Manage.*, vol. 90, pp. 300–314, Jan. 2015, doi: 10.1016/j.enconman.2014.11.033.

[9] *MOBISMART Off-Grid Mobile Power & Storage | Smart Off-Grid Power Technologies | Replace Diesel Generators in Remote Locations With Mobile Clean Power | 855-806-0188*. MOBISMART Off-Grid Mobile Power & Storage. Accessed: May 2, 2020. [Online]. Available: https://mobismart.ca/

[10] S. M. Bragg-Sitton, R. Boardman, and I. N. Laboratory, "Rethinking the future grid: Integrated nuclear renewable energy systems," Nat. Renew. Energy Lab. (NREL), Golden, CO, USA, Tech. Rep. NREL/CP-6A20-63207, Jan. 2015, p. 14.

[11] F. Bienvenu, "Potential of industry for load regulation," Ecole Polytechnique Idaho Nat. Lab., Idaho Falls, ID, USA, 2011.

[12] M. Ruth, D. Cutler, F. Flores-Espino, and G. Stark, "The economic potential of nuclear-renewable hybrid energy systems producing hydrogen," Joint Inst. Strategic Energy Anal., Golden, CO, USA, Tech. Rep. NREL/TP-6A50-66764, 1351061, Apr. 2017, doi: 10.2172/1351061.

[13] M. F. Ruth, O. R. Zinaman, M. Antkowiak, R. D. Boardman, R. S. Cherry, and M. D. Bazilian, "Nuclear-renewable hybrid energy systems: Opportunities, interconnections, and needs," *Energy Convers. Manage.*, vol. 78, pp. 684–694, Feb. 2014, doi: 10.1016/j.enconman.2013.11.030.

[14] S. M. Bragg-Sitton, R. Boardman, C. Rabiti, J. S. Kim, M. Mckellar, P. Sabharwall, J. Chen, M. S. Cetiner, T. J. Harrison, and A. L. Qualls, "Nuclear-renewable hybrid energy systems: 2016 Technology development program plan," Idaho Nat. Lab., Idaho Falls, ID, USA, Tech. Rep. INL/EXT–16-38165, 1333006, Mar. 2016, doi: 10.2172/1333006.

[15] P. Sabharwall, S. Bragg-Sitton, L. Boldon, and S. Blumsack, "Nuclear renewable energy integration: An economic case study," *Electr. J.*, vol. 28, no. 8, pp. 85–95, Oct. 2015.

[16] J. S. Kim, R. D. Boardman, and S. M. Bragg-Sitton, "Dynamic performance analysis of a high-temperature steam electrolysis plant integrated within nuclear-renewable hybrid energy systems," *Appl. Energy*, vol. 228, pp. 2090–2110, Oct. 2018, doi: 10.1016/j.apenergy.2018.07.060.

[17] H. E. Garcia, J. Chen, J. S. Kim, R. B. Vilim, W. R. Binder, S. M. B. Sitton, R. D. Boardman, M. G. McKellar, and C. J. J. Paredis, "Dynamic performance analysis of two regional nuclear hybrid energy systems," *Energy*, vol. 107, pp. 234–258, Jul. 2016, doi: 10.1016/j.energy.2016.03.128.

[18] A. Borisova and D. Popov, "An option for the integration of solar photovoltaics into small nuclear power plant with thermal energy storage," *Sustain. Energy Technol. Assessments*, vol. 18, pp. 119–126, Dec. 2016, doi: 10.1016/j.seta.2016.10.002.

[19] A. Epiney, C. Rabiti, P. Talbot, and A. Alfonsi, "Economic analysis of a nuclear hybrid energy system in a stochastic environment including wind turbines in an electricity grid," *Appl. Energy*, vol. 260, Feb. 2020, Art. no. 114227, doi: 10.1016/j.apenergy.2019.114227.

[20] J. Chen, H. E. Garcia, J. S. Kim, and S. M. Bragg-Sitton, "Operations optimization of nuclear hybrid energy systems," *Nucl. Technol.*, vol. 195, no. 2, pp. 143–156, Aug. 2016, doi: 10.13182/NT15-130.

[21] D. Mikkelson, C.-W. Chang, SacitM. Cetiner, A. L. Qualls, J. M. Doster, and T. N. Dinh, "Small modular reactor modeling using modelica for nuclear-renewable hybrid energy systems applications," Idaho Nat. Lab., Idaho Falls, ID, USA, Tech. Rep. INL/CON-16-39032, Oct. 2015.

[22] Technical Meeting on Nuclear-Renewable Hybdrid Energy Systems for Decarbonized Energy Production and Cogeneration and International Atomic Energy Agency, Eds., *Nuclear-Renewable Hybrid Energy Systems for Decarbonized Energy Production and Cogeneration: Proceedings of a Technical Meeting Held in Vienna*, International Atomic Energy Agency, Vienna, Austria, Oct. 2019, pp. 22–25.

[23] A. S. Epiney, C. Rabiti, P. W. Talbot, J. S. Kim, S. M. Bragg-Sitton, and J. Richards, "Case study: Nuclear-renewable-water integration in Arizona," Int. At. Energy Agency, Vienna, Austria, Tech. Rep. INL/EXT–18-51359-Rev000, 1495196, Sep. 2018, doi: 10.2172/1495196.
[24] J. S. Kim and H. E. Garcia, "Nuclear-renewable hybrid energy system for reverse osmosis desalination process," *Trans. Amer. Nucl. Soc.*, vol. 112, p. 5, Jul. 2015.
[25] M. Ruth, "The economic potential of two nuclear-renewable hybrid energy systems," Joint Inst. Strategic Energy Anal., Golden, CO, USA, Tech. Rep. NREL/TP-6A50-66073, Aug. 2016, p. 275.
[26] E. K. Redfoot and R. A. Borrelli, "Analysis of nuclear renewable hybrid energy systems modeling and nuclear fuel cycle simulators," *Nucl. Technol.*, vol. 204, no. 3, pp. 249–259, Dec. 2018, doi: 10.1080/00295450.2018.1478590.
[27] S. Bragg-Sitton, R. Boardman, M. Ruth, O. Zinaman, C. Forsberg, and J. Collins, "Integrated nuclear-renewable energy systems: Foundational workshop report," Idaho Nat. Lab., Idaho Falls, ID, USA, Tech. Rep. INL/EXT–14-32857-Rev.1, NREL/TP–6A20-62778, 1170315, Aug. 2014, doi: 10.2172/1170315.
[28] *Life-Cycle Emissions–Canadian Nuclear Association*. Accessed: Jul. 5, 2020. [Online]. Available: https://cna.ca/why-nuclear-energy/clean/life-cycle-emissions/
[29] T. Minkiewicz and A. Reński, "Nuclear power plant as a source of electrical energy and heat," Fac. Elect. Control Eng., Gdańsk Univ. Technol., Gdańsk, Poland, Tech. Rep. tom XLI(2011), nr 3-4, 155-166, Oct. 2011.
[30] W. Ko and J. Kim, "Generation expansion planning model for integrated energy system considering feasible operation region and generation efficiency of combined heat and power," *Energies*, vol. 12, no. 2, p. 226, Jan. 2019, doi: 10.3390/en12020226.
[31] *USNC*. Accessed: Dec. 9, 2019. [Online]. Available: https://usnc.com/
[32] M. F. Sherlock, "The renewable electricity production tax credit: In brief," Congressional Res. Service (CRS), Washington, DC, USA, Tech. Rep. R43453, Apr. 2020, p. 16.
[33] *Cost Competitiveness of Micro-Reactors for Remote Markets*. Nucl. Energy Inst., Accessed: Apr. 15, 2019. [Online]. Available: https://www.nei.org/resources/reports-briefs/cost-competitiveness-micro-reactors-remote-markets
[34] A. McDonald and L. Schrattenholzer, "Learning rates for energy technologies," *Energy Policy*, vol. 29, no. 4, pp. 255–261, Mar. 2001, doi: 10.1016/S0301-4215(00)00122-1.
[35] E. S. Rubin, I. M. L. Azevedo, P. Jaramillo, and S. Yeh, "A review of learning rates for electricity supply technologies," *Energy Policy*, vol. 86, pp. 198–218, Nov. 2015, doi: 10.1016/j.enpol.2015.06.011.
[36] Q. Lee, "Learning & experience curves in manufacturing," Strategos, Kansas City, MO, USA, Tech. Rep., 2012, p. 15.
[37] *Latest Oil, Energy & Metals News, Market Data and Analysis | S&P Global Platts*. Accessed: Jul. 13, 2020. [Online]. Available: https://www.spglobal.com/platts/en
[38] G. Locatelli, S. Boarin, F. Pellegrino, and M. E. Ricotti, "Load following with small modular reactors (SMR): A real options analysis," *Energy*, vol. 80, pp. 41–54, Feb. 2015, doi: 10.1016/j.energy.2014.11.040.
[39] *Load Following Power Plant*. Nucl. Power. Accessed: Jul. 13, 2020. [Online]. Available: https://www.nuclear-power.net/nuclear-power/reactor-physics/reactor-operation/normal-operation-reactor-control/load-following-power-plant/
[40] C. Lewis, R. MacSweeney, M. Kirschel, W. Josten, T. Roulstone, and G. Locatelli. (Mar. 2016). *Small modular reactors: Can Building Nuclear Power Become More Cost-Effective?*. National Nuclear Laboratory. [Online]. Available: https://www.researchgate.net/publication/321715136_Small_modular_reactors_Can_building_nuclear_power_become_more_cost-effective
[41] S. Bragg-Sitton, "Hybrid energy systems (HESs) using small modular reactors (SMRs)," in *Handbook of Small Modular Nuclear Reactors*. Amsterdam, The Netherlands: Elsevier, 2015, pp. 319–350.
[42] C. L. Archer and M. Z. Jacobson, "Supplying baseload power and reducing transmission requirements by interconnecting wind farms," *J. Appl. Meteorol. Climatol.*, vol. 46, no. 11, pp. 1701–1717, Nov. 2007, doi: 10.1175/2007JAMC1538.1.
[43] B. Upadhyaya and T. Kerlin, *Dynamics and Control of Nuclear Reactors*, 1st ed. San Diego, CA, USA: Academic, 2019.
[44] *How HOMER Calculates the PV Array Power Output*. Accessed: Nov. 25, 2019. [Online]. Available: https://www.homerenergy.com/products/pro/docs/latest/how_homer_calculates_the_pv_array_power_output.html
[45] P. W. Stackhouse. *Surface Meteorology and Solar Energy (SSE) Data Release 5.1*. Accessed: Jul. 24, 2020. [Online]. Available: https://ntrs.nasa.gov/search.jsp?R=20080012141
[46] N. E. B. Government of Canada. (Feb. 13, 2020). *NEB–Market Snapshot: The Cost to Install Wind and Solar Power in Canada is Projected to Significantly Fall Over the Long Term*. Accessed: Jul. 24, 2020. [Online]. Available: https://www.cer-rec.gc.ca/nrg/ntgrtd/mrkt/snpsht/2018/11-03cstnstllwnd-eng.html
[47] *Solar Panel Maintenance Costs | Solar Power Maintenance Estimates*. Fixr.com. Accessed: Apr. 16, 2020. [Online]. Available: https://www.fixr.com/costs/solar-panel-maintenance
[48] *What Is the Lifespan of a Solar Panel?*. Accessed: Apr. 16, 2020. [Online]. Available: https://www.engineering.com/DesignerEdge/DesignerEdgeArticles/ArticleID/7475/What-Is-the-Lifespan-of-a-Solar-Panel.aspx
[49] S. Diaf, G. Notton, M. Belhamel, M. Haddadi, and A. Louche, "Design and techno-economical optimization for hybrid PV/wind system under various meteorological conditions," *Appl. Energy*, vol. 85, no. 10, pp. 968–987, Oct. 2008, doi: 10.1016/j.apenergy.2008.02.012.
[50] *Small Wind Turbines*. Eocycle. Accessed: Jul. 24, 2020. [Online]. Available: https://eocycle.com/our-wind-turbines/
[51] *US Wind O&M Costs Estimated at $48,000/MW; Falling Costs Create New Industrial Uses: IEA | New Energy Update*. Accessed: Apr. 17, 2020. [Online]. Available: https://analysis.newenergyupdate.com/wind-energy-update/us-wind-om-costs-estimated-48000mw-falling-costs-create-new-industrial-uses-iea
[52] T. Stehly, P. Beiter, D. Heimiller, and G. Scott, "2017 cost of wind energy review," Golden, CO, USA, Nat. Renew. Energy Lab., Tech. Rep. NREL/TP-6A20-72167, 2018. Accessed: May 25, 2020. [Online]. Available: https://www.nrel.gov/docs/fy18osti/72167
[53] *Types of hydropower | International Hydropower Association*. Accessed: Mar. 16, 2020. [Online]. Available: https://www.hydropower.org/types-of-hydropower
[54] (Sep. 25, 2018). *Flows*. Int. Joint Commission. Accessed: Mar. 16, 2020. [Online]. Available: https://ijc.org/en/loslrb/watershed/flows
[55] *How HOMER Calculates the Hydro Power Output*. Accessed: Nov. 25, 2019. [Online]. Available: https://www.homerenergy.com/products/pro/docs/latest/how_homer_calculates_the_hydro_power_output.html
[56] H. A. Gabbar, M. R. Abdussami, and M. I. Adham, "Techno-economic evaluation of interconnected nuclear-renewable micro hybrid energy systems with combined heat and power," *Energies*, vol. 13, no. 7, p. 1642, Apr. 2020, doi: 10.3390/en13071642.
[57] A. Acakpovi, "Original framework for optimizing hybrid energy supply," *J. Energy*, vol. 2016, pp. 1–10, 2016, doi: 10.1155/2016/8317505.
[58] *Renewable Energy Technologies: Cost Analysis Series (Hydropower)*, Int. Renew. Energy Agency (IRENA), Abu Dhabi, United Arab Emirates, Jun. 2012.
[59] *A Geographical Profile of Livestock Manure Production in Canada, 2006*. Accessed: Jul. 23, 2020. [Online]. Available: https://www150.statcan.gc.ca/n1/pub/16-002-x/2008004/article/10751-eng.htm
[60] L. Jarrar, O. Ayadi, and J. Al Asfar, "Techno-economic aspects of electricity generation from a farm based biogas plant," *J. Sustain. Develop. Energy, Water Environ. Syst.*, vol. 8, no. 3, pp. 476–492, Sep. 2020, doi: 10.13044/j.sdewes.d7.0302.
[61] *Biogas Basics–Energypedia.Info*. Accessed: Jul. 23, 2020. [Online]. Available: https://energypedia.info/wiki/Biogas_Basics
[62] M. Lantz, "The economic performance of combined heat and power from biogas produced from manure in Sweden–A comparison of different CHP technologies," *Appl. Energy*, vol. 98, pp. 502–511, Oct. 2012, doi: 10.1016/j.apenergy.2012.04.015.
[63] German Solar Energy Society (DGS), *Planning and Installing Bioenergy Systems: A Guide for Installers, Architects and Engineers*, 1st ed. Evanston, IL, USA: Earthscan Publications Ltd., 2004.
[64] Y. R. Chen, "Thermal properties of beef cattle manure," *Agricult. Wastes*, vol. 6, no. 1, pp. 13–29, May 1983, doi: 10.1016/0141-4607(83)90003-3.
[65] H. M. Morgan, W. Xie, J. Liang, H. Mao, H. Lei, R. Ruan, and Q. Bu, "A techno-economic evaluation of anaerobic biogas producing systems in developing countries," *Bioresource Technol.*, vol. 250, pp. 910–921, Feb. 2018, doi: 10.1016/j.biortech.2017.12.013.
[66] P. Lako. (May 2010). *Biomass for Heat and Power*. Energy Technology Systems Analysis Program (ETSAP). [Online]. Available: https://iea-etsap.org/

[67] H. S. Das, C. W. Tan, A. H. M. Yatim, and K. Y. Lau, "Feasibility analysis of hybrid photovoltaic/battery/fuel cell energy system for an indigenous residence in east malaysia," *Renew. Sustain. Energy Rev.*, vol. 76, pp. 1332–1347, Sep. 2017, doi: 10.1016/j.rser.2017.01.174.
[68] A. Fathy, "A reliable methodology based on mine blast optimization algorithm for optimal sizing of hybrid PV-wind-FC system for remote area in egypt," *Renew. Energy*, vol. 95, pp. 367–380, Sep. 2016, doi: 10.1016/j.renene.2016.04.030.
[69] A. M. Abdelshafy, H. Hassan, A. M. Mohamed, G. El-Saady, and S. Ookawara, "Optimal grid connected hybrid energy system for egyptian residential area," in *Proc. Int. Conf. Sustain. Energy Eng. Appl. (ICSEEA)*, Oct. 2017, pp. 52–60, doi: 10.1109/ICSEEA.2017.8267687.
[70] (Jan. 2, 2019). *Efficiency Water Electrolysis*. DeepResource. Accessed: Jul. 24, 2020. [Online]. Available: https://deepresource.wordpress.com/2019/01/02/efficiency-water-electrolysis/
[71] S. Kharel and B. Shabani, "Hydrogen as a long-term large-scale energy storage solution to support renewables," *Energies*, vol. 11, no. 10, p. 2825, Oct. 2018, doi: 10.3390/en11102825.
[72] *California Hydrogen Business Council–CHBC–Hydrogen Means Business in California*. Accessed: Jul. 24, 2020. [Online]. Available: https://www.californiahydrogen.org/
[73] H. Borhanazad, S. Mekhilef, V. Gounder Ganapathy, M. Modiri-Delshad, and A. Mirtaheri, "Optimization of micro-grid system using MOPSO," *Renew. Energy*, vol. 71, pp. 295–306, Nov. 2014, doi: 10.1016/j.renene.2014.05.006.
[74] *PV Performance Modeling Collaborative | CEC Inverter Test Protocol*. Accessed: Jul. 24, 2020. [Online]. Available: https://pvpmc.sandia.gov/modeling-steps/dc-to-ac-conversion/cec-inverter-test-protocol/
[75] X. Luo, J. Wang, M. Dooner, and J. Clarke, "Overview of current development in electrical energy storage technologies and the application potential in power system operation," *Appl. Energy*, vol. 137, pp. 511–536, Jan. 2015, doi: 10.1016/j.apenergy.2014.09.081.
[76] (Jan. 2013). *Thermal Energy Storage Technology Brief*. IEA-ETSAP IRENA Technol. Brief E17. [Online]. Available: https://www.irena.org/publications/2013/Jan/Thermal-energy-storage.
[77] W.-D. Steinmann and M. Eck, "Buffer storage for direct steam generation," *Sol. Energy*, vol. 80, no. 10, pp. 1277–1282, Oct. 2006, doi: 10.1016/j.solener.2005.05.013.
[78] Technology Roadmap Energy Storage. (2014). *INTERNATIONAL ENERGY AGENCY, 9 Rue de la Fédération 75739 Paris Cedex*, vol. 15, France. [Online]. Available: https://speicherinitiative.at/assets/Uploads/20-technologyroadmapenergystorage.pdf
[79] *LION ELECTRIC BOILER 28KW | Boilers | Northern Hydronics*. Accessed: Apr. 24, 2020. [Online]. Available: http://www.northernhydronics.com/Boilers/LION-ELECTRIC-BOILER-28KW/flypage.tpl.html?pop=0
[80] *Are Electric Boilers Better Than Gas Boilers?–VHL*. Village Heating LTD Facilities. Accessed: Oct. 30, 2015. [Online]. Available: https://www.villageheating.co.uk/alternate-heating-are-electric-boilers-better-than-gas-boilers/
[81] *Learn How Much it Costs to Install a Steam Shower or Steam Room*. Accessed: Apr. 24, 2020. [Online]. Available: https://www.homeadvisor.com/cost/plumbing/steam-shower-installation/
[82] *Combined Heat and Power Technology Fact Sheet Series*. US Department of Energy. Accessed: Apr. 24, 2020. [Online]. Available: https://betterbuildingssolutioncenter.energy.gov/sites/default/files/attachments/CHP-Steam%20Turbine.pdf
[83] *Electricity Generating and Distribution Efficiency*. Accessed: Jul. 24, 2020. [Online]. Available: https://www.mpoweruk.com/energy_efficiency.htm
[84] *A-to-Z Guide to Thermodynamics, Heat and Mass Transfer, and Fluids Engineering: AtoZ*, Begellhouse, New York, NY, USA, 2006.
[85] (Jun. 01, 2007). *Steam Generator Efficiency*. Power Eng., Accessed: Jul. 24, 2020. [Online]. Available: https://www.power-eng.com/2007/06/01/steam-generator-efficiency/
[86] R. K. Rajkumar, V. K. Ramachandaramurthy, B. L. Yong, and D. B. Chia, "Techno-economical optimization of hybrid pv/wind/battery system using neuro-fuzzy," *Energy*, vol. 36, no. 8, pp. 5148–5153, Aug. 2011, doi: 10.1016/j.energy.2011.06.017.
[87] C.-T. Tsai, T. M. Beza, W.-B. Wu, and C.-C. Kuo, "Optimal configuration with capacity analysis of a hybrid renewable energy and storage system for an island application," *Energies*, vol. 13, no. 1, p. 8, Dec. 2019, doi: 10.3390/en13010008.
[88] R. Luna-Rubio, M. Trejo-Perea, D. Vargas-Vázquez, and G. J. Ríos-Moreno, "Optimal sizing of renewable hybrids energy systems: A review of methodologies," *Sol. Energy*, vol. 86, no. 4, pp. 1077–1088, Apr. 2012, doi: 10.1016/j.solener.2011.10.016.
[89] *Salvage Value*. Accessed: Jul. 13, 2020. [Online]. Available: https://www.homerenergy.com/products/pro/docs/latest/salvage_value.html
[90] C. M. Martínez and D. Cao, "Integrated energy management for electrified vehicles," in *Ihorizon-Enabled Energy Management for Electrified Vehicles*. Amsterdam, The Netherlands: Elsevier, 2019, pp. 15–75.

HOSSAM A. GABBAR (Senior Member, IEEE) received the B.Sc. degree (Hons.) from the Faculty of Engineering, Alexandria University, Egypt, in 1988, and the Ph.D. degree from Okayama University, Japan, in 2001. From 2001 to 2004, he joined the Tokyo Institute of Technology, as a Research Associate. From 2004 to 2008, he joined Okayama University, as a Tenured Associate Professor. From 2007 to 2008, he was a Visiting Professor at the University of Toronto. He is a Professor with the Faculty of Energy Systems and Nuclear Science, Ontario Tech University (UOIT), and was cross appointed at the Faculty of Engineering and Applied Science. He has established the Energy Safety and Control Laboratory (ESCL). He is a leading national and international researcher in the areas of smart energy grids and resilient transportation electrification. He was a recipient of the Senior Research Excellence Award in 2016 with more than 220 publications.

MUHAMMAD R. ABDUSSAMI received the bachelor's degree in electrical and electronics engineering from the Islamic University of Technology (IUT), Bangladesh. He is currently pursuing the M.A.Sc. degree in nuclear-renewable hybrid energy system with the Faculty of Energy Systems and Nuclear Science, Ontario Tech University (UOIT), Canada. He is very passionate about the innovation of nuclear-renewable micro hybrid energy systems and energy management. His research interests include nuclear power, renewable energy, smart energy grid, nuclear-renewable integration systems, and energy storage systems.

MD. IBRAHIM ADHAM received the bachelor's degree in electrical and electronics engineering from the Islamic University of Technology (IUT), Bangladesh. He is currently pursuing the master's degree in nuclear engineering with the Faculty of Energy Systems and Nuclear Science, Ontario Tech University (UOIT), Canada. He is working on nuclear-renewable integrated system for marine ships. His research interests include nuclear power, renewable energy, smart grid, and fast charging station for electric vehicles.